FINAL TECHNICAL REPORT
PROJECT A-627

44p.

A SUBMILLIMETER INTERFERENCE SPECTROMETER

N64-29193
(ACCESSION NUMBER) 44 (PAGES) (THRU)
Cr-56839 (NASA CR OR TMX OR AD NUMBER) 15 (CODE) (CATEGORY)
FACILITY FORM 602

BY Wayne K. Rivers, Jr

Sponsored by
The National Aeronautics and Space Administration
Under Research Grant NsG-258-62

Report submitted to NASA for consideration for Publication as
a NASA Technical Note

8 May

Engineering Experiment Station
GEORGIA INSTITUTE OF TECHNOLOGY
Atlanta, Georgia

UNPUBLISHED PRELIMINARY DATA

XEROX $ 4.60 ph
MICROFILM $ ____
OTS PRICE

PC # 2

NATIONAL AERONAUTICS AND SPACE ADMINISTRATION

TECHNICAL NOTE

A SUBMILLIMETER INTERFERENCE SPECTROMETER

By Wayne K. Rivers, Jr.

29,93

SUMMARY

The principles of operation and construction of an interference spectrometer which is intended to be used in the shorter millimeter and submillimeter region are discussed. The instrument, which uses a wavefront dividing interferometer, has high resolving power for this region of the spectrum, one part in 500, making it especially useful at the longer wavelengths.

Problems in the development of the instrument, including the mechanical design of the interferometer drive and the fabrication of microwave-optical elements peculiar to the instrument, are discussed.

The results of limited tests performed are discussed. Included are spectra of a monochromatic source with a spectral resolution of 0.011 cm^{-1} (330 mc) and the transmission of a high-pass filter with spectral resolution of about 0.03 cm^{-1}.

Cust h

INTRODUCTION

Instrumentation for the region of the electromagnetic spectrum with wavelengths of a few tenths of millimeters to a few millimeters is difficult to realize because many of the techniques used in the optical and infrared region and in the microwave region of the spectrum are nonexistent or have serious shortcomings when applied to the middle ground between the two. For example, neither the coherent sources common at microwaves nor the relatively narrow discrete line spectra of the visible are available for use as signal sources in the submillimeter region. Extensive tube development and quantum mechanical generator research programs are now being sponsored and should in time provide sources of monochromatic power and sensitive receivers in this region. However, techniques employing broadband radiation sources, spectrometers, and direct detectors, such as the crystal rectifier and thermal types, will continue to provide the data on materials and components necessary for the eventual utilization of the submillimeter region of the spectrum (ref. 1).

The most common type of far infrared spectrometer uses a reflection grating to filter a "white" source of radiation. Long and intensive

development of the grating spectrometer has provided solutions for such problems as loss of energy into unwanted reflection orders and the passing of harmonically related wavelength bands, so that complete monochrometer systems are commercially available at infrared and shorter wavelengths. At present, specially designed instruments must be constructed for wavelengths much longer than 100μ. The submillimeter instruments at Syracuse University (ref. 2), New York University (ref. 3), Osaka University (ref. 4), and University of Frankfurt (ref. 5) are examples of this long-used type of spectrometer.

Relatively recently, Strong (ref. 6) and others (refs. 7 and 8) have applied the principle of interference modulation to the design of a radically different spectrometer. In this scheme an incoming wave is divided into two equal components which propagate over paths of variable path length before being recombined and detected. When the relative path length traversed by the wave components is varied continuously, the amplitude of the combined wave is modulated at a rate which depends on the wavelength of the radiation and the rate of change of relative path length. There is a one-to-one correspondence between the radio frequency spectra present in the radiation and the amplitude modulation spectra produced. Thus, a spectral analysis of the audio output of the spectrometer detector is a representation of the radio-frequency spectrum.

In general, interference spectrometers have the advantage of high radiant efficiency difficult to obtain with grating spectrometers. In the latter, means must be included to remove unwanted radiation reflected at higher orders than the desired one, and the use of frequency selective choppers and reststrahlen filters is common. The interference spectrometer offers almost complete freedom from unwanted responses. For linear relative motion of the interferometer mirrors, each radio frequency is modulated at a different audio rate, and little, if any, prefiltering is required.

Interference modulation spectrometers offer the capability of greater resolution than can be conveniently obtained with grating instruments. In both types of spectrometers, the resolving power is proportional to the number of wavelengths which interfere. For example, the resolving power of an optical-type grating is the product of the number of lines in the grating and the order, which is the number of wavelengths phase difference between rays reflected from adjacent lines. In the interference modulation spectrometer, the resolving power is the number of wavelengths of path difference introduced in one wave component with respect to the other. This path difference can be very large, and resolution would always be sensitivity limited.

The geometries which have been used for interference spectrometers are the Twyman-Green interferometer (see ref. 8 and Appendix B of ref. 10), a modified Michelson type, and a lamellar grating (refs. 6 and 7) in a Czerny-Turner mounting in which a pair of interleaved gratings move with

respect to each other. In the former case, two beams are formed and handled separately in the optics. In the latter design, the two moving reflecting surfaces form one unit, and only a single beam is used.

This report concerns the development of an interference spectrometer which is intended to be used over the wavelength range of 100μ to 4 mm. An unusual feature of the instrument is its high resolving power for these long wavelengths, about 250 at 4 mm increasing to a maximum of 500 at shorter wavelengths. The corresponding absolute spectral resolution is quite small, a minimum of 0.01 cm^{-1}. Because it is intended that the instrument serve not only as a tool for basic research but also as a vehicle for the development of submillimeter techniques, a somewhat unusual configuration was chosen which combines optical and microwave techniques. It is this unusual configuration which allows a long relative path difference to be introduced in the interferometer, resulting in the small absolute spectral resolution referred to above.

This report describes the configuration of the instrument, features of its operation which are peculiar to this configuration, some of the problems in the development of the instrument, and the data recording and processing techniques used. Test results are given for the wavelength region in the neighborhood of 4 to 7 mm, because it was only in this region that a high temperature noise source and sensitive bolometer were available which were suitable for the tests.

SYMBOLS

$A( )$	apodizing function
$B( )$	calculated spectrum power density
B_v	post-detection integration bandwidth
c	speed of propagation
D	diameter of mirror aperture
$E( )$	field amplitude
j	integer index
k	Boltzmann's constant
L	maximum value of x
M	index denoting zero point of interferogram

N	number of points in interferogram
NEP	noise-equivalent power
P( )	power
R	responsivity of square-law detector (volt per watt)
S/N	signal-to-noise ratio
T	temperature
t	time
V( )	output voltage of square-law detector; interferogram function
x	relative path length difference
Γ	interferometer transmission factor
δ	mirror displacement
λ	wavelength
ν	frequency (cps)
ϕ	phase angle (radian)
τ	time constant
ω	frequency (radian per sec) = $2\pi\nu$

Unit Abbreviations:

μ	micron
mm	millimeter
cm	centimeter
m	meter
mc	megacycle per second
gc	gigacycle per second
degK	degree Kelvin

db decibel

Notation:

1.38^{-23} implies 1.38×10^{-23}

I. DESCRIPTION OF INSTRUMENT

Principle of Operation

The purpose of a spectrometer is to provide information about the power density spectrum of radiation from a broadband source as modified perhaps by an intervening absorbing medium. An interference spectrometer does this by recording the longitudinal spatial correlation function of the electromagnetic wave from which the spectrum can be calculated by fourier transformation. It is not desirable to present here a detailed theory of interference spectroscopy. Detailed theoretical treatments are available in the works of Strong (ref. 9 and Appendix F of ref. 10), Genzel (ref. 11) and Connes (ref. 12). However, a brief review of the interference modulation process will be presented in order that the essential operating features of the spectrometer can be related.

In figure 1 a two-beam interferometer is depicted schematically. The basic elements of this interferometer are a means of dividing the radiation into two paths, a means of changing the differential path length, and a means of recombining the two wave components. Auxiliary components necessary are a broadband energy source and a square-law detector. This detector responds to the total power incident upon it; let its responsivity, R, in units of volts per watt, be uniform over the input band. The power incident on the detector is the sum of two partial waves with amplitudes $E(\omega)$ in a spectral interval $(\omega, \omega+d\omega)$, one of which is delayed with respect to the other by a distance x or angle $x\omega/c$. Thus the detector response, $V(x)$, as a function of the path delay, x, is

$$V(x) = R \int \overline{[E(\omega)\ \cos\omega t + E(\omega)\ \cos(\omega t + x\omega/c)]^2}\ d\omega \quad , \qquad (1)$$

where c is the effective velocity of propagation in the delay paths and the bar implies time averaging. Note that $V(x)$, which is called the interferogram, is symmetrical in the path delay, x. By applying simple trigonometric identities, the interferogram can be put in the form

$$V(x) = \frac{R}{2}\int P(\omega)\cos(x\omega/c)\,d\omega + \text{constant terms}, \qquad (2)$$

where $P(\omega) = [E(\omega)]^2$. It is evident from this equation that $V(x)$ is proportional to the cosine fourier transform of $P(\omega)$. Thus $P(\omega)$ must be proportional to the inverse cosine fourier transform of $V(x)$,

$$P(\omega) \propto \int V(x)\cos(x\omega/c)\,dx \quad . \qquad (3)$$

Because the integral in equation (3) is symmetric in the path delay, x, the power spectrum $P(\nu)$, $\nu = \omega/2\pi$, is completely determined by an interferogram defined only over the interval $0 \leq x \leq \infty$, and recording of $V(x)$ is not necessary for negative x. In practice the interferogram can be recorded only over a finite interval $0 \leq x \leq L$. The consequence of this limitation is that the spectral resolution is then also finite and is given approximately by

$$\Delta\nu \approx c/L \quad . \qquad (4)$$

The process of using the interference spectrometer then is one of recording the output of the detector at regular intervals of the mirror displacement and taking the numerical fourier transform of these data to obtain the power spectrum of the detected radiation. The effect of this process on resolution is further discussed along with apodization and problems associated with location of the point $x = 0$ in chapter III. The available signal-to-noise ratio for an interference spectrometer is also discussed in chapter III in connection with the results obtained for the particular source and detector used in the tests.

The Georgia Tech Interferometer

The configuration chosen for the spectrometer is illustrated in plan view in figure 1, and a photograph of the system is shown in figure 2. The path taken by the radiation through the system is illustrated by the dotted lines in figure 1. Radiation from the noise source (S) is passed through a short section of dominant (TE_{10}) mode waveguide to a waveguide horn (H1). The spherical wavefront is reflected by the prolate-spheroidal reflector (R1) to another reflector (R2), through a hole in the mirror (M1) onto the

paraboloid (P1). The plane wave off this paraboloid is changed in direction by the mirror (M1) and is split in a vertical plane by the 90 degree mirror pair (M2-3). The two partial waves, which are now travelling in opposite directions are reversed in direction of travel by the dihedral mirrors (DM1, DM2) and returned to the second 90 degree mirror pair (M4-5) where the partial waves are recombined into a continuous plane wave. This plane wave after reflection from mirror (M6) is focused by the paraboloid (P2) onto a waveguide horn (H2) in a hole in mirror (M6). This horn is connected by another short length of dominant mode rectangular waveguide to the detector (D).

The relative path length travelled by the two partial plane waves is changed by moving the two dihedral mirrors (DM1,2), which are mounted on a common base or slide. It is seen that differential path distance is introduced at four times the rate of motion of the slide.

Suppose that the slide is positioned such that at a given frequency the differential path length is an odd number of half wavelengths. Then the spherical wave incident on the detector horn (H2) will have a phase difference of 180 degrees between the right half of the wave and the left half. Since the horn responds only to a symmetric spherical wave, it will not accept this antisymmetric wave, and the energy will be reradiated (reflected). Let the wave containing two parts, one of which is delayed with respect to the other, be represented by the equal amplitude components

$$E_r = E \cos (\omega t + \phi/2)$$

$$E_l = E \cos (\omega t - \phi/2) \quad , \tag{5}$$

where $\phi = 2\pi \cdot 4\delta/\lambda$, and δ is the slide displacement from the symmetric or central maximum position. By expanding the wave into symmetric and antisymmetric components,

$$E_s = (E_r + E_l)/2$$

$$E_a = (E_r - E_l)/2 \tag{6}$$

and substituting equation (5), one obtains

$$E_s = E \cos \omega t \cos(\phi/2)$$

$$E_a = -E \sin \omega t \sin(\phi/2) \quad . \tag{7}$$

The powers in these symmetric and antisymmetric components are

$$P_s = \frac{E^2}{2} \cos^2 \frac{\phi}{2} \tag{8a}$$

$$P_a = \frac{E^2}{2} \sin^2 \frac{\phi}{2} \quad . \tag{8b}$$

Equation (8a) has the form of the intensity at the output of a general two-path interferometer (section 8-3 of ref. 10), and it is of the correct form to ensure that the process described by equation (2) is valid.

The process described above in which a symmetrical plane wave is sheared by the interferometer delay system into an antisymmetric plane wave reveals a disadvantage of this type of wavefront dividing interferometer. That is, if an antisymmetric wave is launched from the source, it will be converted into a symmetric wave on the exit side, and vice versa. Thus, if one attempts to use an extended area source or detector with this interferometer, that is, either a source or detector which excites or accepts both symmetric and antisymmetric modes, interference modulation may not be observed, for the power received by the detector will be a constant, on the average, as a function of path delay. In order that the desired interference modulation take place, energy should enter the interferometer in a single spatial mode, in this case a plane TEM wave launched from dominant mode waveguide.

II. DEVELOPMENT

Model Interferometer

In order to verify the predicted characteristics of the wavefront dividing interferometer, it was modelled at 15 gc for testing with a klystron signal source. A photograph of the mock-up is shown in figure 3. A comparison of the important parameters and experimental results for the model and the final form of the spectrometer is made in table I. Experiments on the model with a c-w source provided confirmation of the predicted behavior of plane waves in the interferometer and allow the following conclusions:

1. Energy can be transferred from one waveguide terminal to another in a plane-wave mode formed by parabolic mirrors over distances of the order of 0.1 D^2/λ, where D is the paraboloid diameter, with loss as low as 1.2 db. The investigations have established qualitative understanding of the factors affecting the launching and recovery losses for plane waves. These are discussed in detail later in this chapter.

2. Introduction of the plane mirror "maze" between the paraboloids increased the transmission loss by 2.5 db for both polarizations in the model. This loss is attributable to diffraction at the edge of beam splitter and dihedral reflectors where the field intensity is a maximum. This loss should depend on the size of the aperture in units of D^2/λ and thus for a given aperture size will be smaller at shorter wavelengths.

3. The wavelength in the interferometer differs from the free space wavelength by an amount depending on the polarization. This shift is caused by the restriction of the wave to finite transverse dimensions. In the model the shift was about 0.3 per cent for the most unfavorable polarization, the E field vertical, and about half that amount for the other polarization. Using simple dominant-mode (TE_{10}) waveguide correction, shifts of 0.22 and 0.06 per cent would be predicted. In the final model, horizontal polarization is used, and a range of shift of 90 to less than 0.1 part per million for the wavelength range of 4 mm to 0.1 mm (100μ) is expected.

4. The wavelength in the 15 gc model was uniform for increases in the path length of one of the half-beams of about 80 cm within the resolution of the measurements, about 5 parts in 10,000. Variation in the wavelength with path length delay is equivalent to introducing phase error in the fourier transformation. If the maximum resolution of the final instrument of 0.01 cm^{-1} were required at a wavelength of 0.1 mm, a constancy of the wavelength in the variable delay paths of about 25 parts in a million would be required. Since a total shift from free space wavelength of less than this is predicted, no problem due to wavelength variation is expected.

5. The output of the detector as a function of mirror position when the model interferometer was excited by a continuous wave source was a sine wave with distortion products which were about 25 db below the fundamental. The principal harmonic component was the third, and it was produced by energy in the interferometer which was reflected from the detector horn, passed back to the source horn, reflected at the source, and received after the third traverse of the interferometer. Doubtless other odd harmonics were produced by this process but they were not analyzed. The limitation of this multiple reflection distortion on the operating range of the spectrometer to a 3:1 frequency range is not serious because a given set of terminal waveguide horns will of themselves limit useful operation to about a 2:1 ratio of frequencies.

Mechanical Design

The principal mechanical problem in the design of the interference spectrometer was the provision of a linear translation mechanism for the two dihedral mirrors. Coupled with the problem of providing mirror motion is that of synchronization of the data sampling and recording with the mirror position. Desirable characteristics that this drive should possess are listed below:

1. Traverse the dihedral mirror pair 25 cm for total path delay of 1 meter.

2. Linearity in the position of the mirror slide to the point in the drive at which data sampling impulses are derived within ±2.5μ (±0.0001 inch) over the 25 cm. Alternately, provision for use with an auxiliary standard of length for deriving the sampling impulses (for example, an optical interferometer and fringe counter).

3. Smoothness of the drive adequate to operate optical fringe counter.

4. Control of speed of drive in suitable steps for recording sampled data over the wavelength range of 4 mm to 0.1 mm.

Since a drive screw with the desired accuracy which could provide both functions of translating the mirrors and generating accurate data sampling control pulses could not be obtained for a reasonable amount of money, the concept was allowed of a separate drive mechanism which was smooth, but possibly inaccurate, and a length standard which would produce sampling control pulses at precise increments of mirror position. One of the drive mechanisms investigated was a hydraulic system consisting of a hydraulic cylinder whose piston was rigidly coupled to the mirror slide. The cylinder discharged through a very small (0.002 to 0.005 inch diameter) sharp-edged orifice. The inlet side of the cylinder was fed from an accumulator which was charged with high-pressure regulated nitrogen in the range 500 to 1500 psi. Tests made on a mock-up of a mirror drive system with a 4 inch diameter cylinder revealed the following problems:

A. It was difficult to remove all air bubbles from the lines and cylinder, so that the ultimate stiffness of the system could not be realized.

B. Next to bubble compression, stiffness was limited by the length expansion of the discharge line, which would have to be of considerable wall thickness to achieve a suitable stiffness.

C. The necessary friction contact between piston and cylinder walls and end seals produced appreciable stiction which, in combination with the reduced stiffness of the system, produced jerky motion of an order much

greater than tolerable since an optical type fringe counter would be required with this form of drive.

D. Operating controls and maintenance requirements appeared to be excessive for routine convenient operation.

The combination of our brief experience with the above test hydraulic system, descriptions of other hydraulic approaches (e.g. see ref. 13), and limited funding dictated a "safe", although compromising approach, using a lead screw drive which could perform both functions of data sampling control and mirror translation, but with reduced accuracy.

In principle a mechanical lead screw possesses disadvantages analogous to some of the above factors, but in practice the state of development of screws is such as to result in a stiffer, smoother and easier-to-use drive with far less development effort and maintenance. The configuration which was chosen uses a cast aluminum base or "slide" which supports the two dihedral mirrors. This slide rides on two granite rails, a principal one 6 feet long by 3 inches wide, and an outrigger 2 feet by 2 inches. These rails are commercial granite parallels with working surfaces flat to ±20 μinch. The slide rolls on recirculating roller bearings which have a specified uniformity of 25 μinch. Motion of the slide is produced by an 0.5 inch diameter recirculating ball screw with a pitch of 0.0625 inch with absolute maximum error specified to be less than one part in 2000 over its useful length of 20 inches. The combination of these components has resulted in an interferometer drive which will allow a fractional spectral resolution of about one part in 500 over the wavelength range of 0.1 mm to 2 mm, and a resolution at longer wavelengths which is limited by the maximum mirror stroke of 25 cm (path delay difference of 1 meter). Mechanical tests of the drive indicate that the small scale slow speed accuracy is limited to about ±50 μinch by springiness in the screw driveshaft couplings and screw thrust bearing supports. Considerable improvement is expected when these parts are beefed up, which can be accomplished in the event that a tighter drive is required for use with a fringe counter for data sampling control. This would only be required if fractional resolution less than one part in 500 is demanded.

Optical Elements and Errors

The principal optical elements used in the spectrometer are two 2-1/2 inch aperture prolate spheroidal reflectors, two 12 inch f:1 paraboloids, and 10 flat mirrors. In traversing the spectrometer from the entrance horn to the exit horn, the energy is reflected from 10 surfaces. If one arbitrarily requires that the total phase error due to incorrect surface contour of the optical elements be less than $\lambda/10$, and assumes that this error is equally distributed among the surfaces randomly, then each surface is required to have an accuracy of 3μ to be useful at the shortest design wavelength of 0.1 mm.

The flat mirrors are made of 1/4 inch thick commercial grade Libby-Owens-Ford Parallel-O-Plate which was coated with 2.5μ of evaporated aluminum. By selecting the best of about a dozen sheets of glass from which to cut the mirrors, plane reflectors were obtained which when standing free on edge were flat to within better than one fringe of light per inch along the surface, thus satisfying the tolerance allowed above.

Both the prolate spheroidal reflectors and 12 inch f:1 paraboloids depart drastically from the simple plane or spherical surfaces generally figured by optical techniques, and yet for this instrument the accuracy requirements are too severe for the application of conventional machining techniques. Although the accuracy required was crude compared to the usual optical standards, the difficulty of figuring these aspherical surfaces was reflected in the high prices and long delivery times quoted by conventional optical sources. Little encouragement was given that the prolate spheroids could be made at all. The high total costs indicated for these reflectors made consideration of a compromise of requirements or the application of unconventional techniques attractive. In particular, it appeared feasible to do a reasonable amount of speculative investigation on a new technique of reflector fabrication.

The required 12 inch diameter f:1 paraboloids were designed and fabricated at Georgia Tech by a novel method. A complete description of these reflectors and the method of fabrication is given in the next section. These reflectors have been tested by simple optical techniques with inconclusive results. The error of surface contour is certainly no greater than ±12μ (0.0005 inch), but it has not been possible to define the accuracy closer. This is because the test definition seems to be limited by the small scale optical polish on the soft aluminum surface rather than the gross surface contour.

The prolate spheroid reflectors were machined on a lathe from aluminum plate by feeding coordinates to cross and axial feeds. They are known to deviate from the desired surface by as much as ±0.001 inch (25μ). For operation of the spectrometer at wavelengths much shorter than 1 mm, these reflectors may have to be replaced with ones having improved accuracy. The placement of these reflectors is shown in the close-up photo of figure 4. They provide a beam region of focal ratio about f:2.5 for introduction of solid absorption samples and short gas cells. The beam dimensions in this region are about 6 cm diameter at each end with a clear length of 20 cm.

The optical elements which are adjustable in position are the four flat mirrors which divide and recombine the plane wave in the interferometer and the paraboloids. The former are adjustable in angular orientation only, and the latter in both elevation and azimuth angles and translation along three axes. The movable dihedral mirrors and the large 45° mirrors are positioned in fixed mounts. The prolate spheroid which is just behind the large 45° mirror is fixed in position and its twin is adjustable with

respect to the source feed horn. Alignment of the elements of the spectrometer is not difficult provided the precaution is taken initially to align the system optically with a point-source light before beginning the process of touching up the adjustments for minimum transmission loss.

Component Development

Twelve-inch Paraboloids.- The f:1 paraboloids were constructed by replicating a machined stainless steel mandrel as shown in figure 5a. This male parabolic surface was machined in a carefully annealed billet of 17-4PH stainless in the following manner. The cylindrical billet, approximately 30.5 cm in diameter by 10 cm high, was mounted on a spindle which was supported by a trunnion bearing. The trunnion was mounted on a sliding table of a vertical mill so that the direction of travel or feed was in the plane of the spindle axis and normal to the trunnion axis. The vertical axis mill cutter was a cylindrical one cutting on its side tangent to the parabolic surface. The parabolic coordinates were specified in a spherical-polar coordinate system in which the spindle was the polar axis and symmetry axis of the paraboloid, and the polar angle (angle between polar axis and point of tangency with mill cutter) was generated by rotations about the trunnion axis. The radial coordinate was fed as a correction to the 24 inch central radius of curvature. This correction to the radius was read by a dial indicator accurate to ±25 μinches, and it ranged over about 0.012 inch (0.3 mm) for the f:1 paraboloid. The machining was performed by Schwartz Boring Company of Detroit, Michigan, and they indicate the mandrel surface to be within ±50 μinches of the desired contour.

It was originally intended that the mandrel be replicated by electroforming copper on the surface, bonding this copper to a support structure, and then separating the copper from the mandrel. Tests on small stainless steel samples indicated difficulty in parting the copper from the stainless. Surface treatments consisting of silicone grease, aquadag and similar contaminant release coatings, and mild surface etches were tested. Those treatments which allowed the plating to be removed from the test samples with reasonable levels of stress had allowed the copper to partially pull away from the steel during the plating so that accurate replication was not accomplished. No satisfactory chemical parting treatment was found, and it was not feasible to establish an adequate evaporation facility to apply the techniques successfully used by others (ref. 14). Efforts to use the electroforming replication technique were postponed, and an alternate method was used.

The foil-transfer replication technique is illustrated in figures 5b and 5c. A sheet of soft aluminum foil about 0.001 inch thick is mounted in an aluminum ring frame. This frame is pulled down around the mandrel so that the foil is stretched in contact with the parabolic surface of the mandrel. In figure 5b the foil has been only partially stretched. The

mandrel and foil are then inverted over the backing structure of the reflector as in figure 5c. The mandrel is then lowered slowly into the backing structure in which an epoxy* adhesive has been poured so that excess adhesive is displaced outward from the center forming a uniform adhesive bond. After room temperature curing for 24 hours, the mandrel is removed and the foil trimmed, resulting in the reflector shown in figure 5d.

The backing for the foil is slip-cast fused silica, which has previously been applied to the construction of optical mirrors (Appendix 1 of ref. 15)**. These structures were cast against plaster molds which were cast against the mandrel by a two-step process. The silica blanks had rather poor accuracy because of considerable shrinkage of the female and male plaster replicas against which the silica slip was cast, and because of slight shrinkage of the silica in firing. The discrepancy between the shape of the silica blank and the foil replica of the stainless steel mandrel is made up by the varying epoxy adhesive thickness. This nonuniformity of adhesive thickness is expected to be a major factor in the accuracy and stability of reflectors made by this process.

Testing of these reflectors is as difficult as the general problem of construction. The gross contour accuracy is probably better than a level conveniently measurable by conventional mechanical techniques, yet the fine grained surface of the aluminum foil is such as to make accurate testing by optical methods difficult. A longitudinal aberration test performed by masking off rings on the surface was limited to about 0.0005 inch (12μ) equivalent surface error in resolution, and within this resolution the surface has the desired contour. Because of limited knowledge and technique of polishing soft aluminum foil, the resolution of this test is the best we have achieved. When a better polishing technique is learned, improved accuracy of the optical measurements can be achieved.

Feed Horns.- It is often desirable to launch an electromagnetic wave from a waveguide, focus it into a plane wave of limited cross section, and recover the energy in the near field of the transmitting terminal in another waveguide with low overall transmission loss. The spectrometer being discussed is an example of such an instance. The design requirements set by this task on the necessary microwave optical elements, which are focusing lenses or reflectors and waveguide horn terminations, are different from those encountered in attaining optimum antenna characteristics in the far field with the same devices. The following requirements must be met for low-loss transmission between large apertures in the near field:

---

*Shell Chemical Company Epon 815 with Curing Agent U.

**Appendix 1 of reference 15 describes work on slip-cast fused silica mirrors performed for Perkin-Elmer Corporation by the High Temperature Materials Branch, Engineering Experiment Station, Georgia Institute of Technology.

1. The concept of impedance matching must be satisfied at each point of the wave. That is, at every point in a plane normal to the axis of the system, the direct wave must have a complex amplitude which is the conjugate of that of the reciprocal wave (one for transmitting and receiving terminals reversed). If the terminals are to be identical, this requirement reduces to the necessity of identically equal amplitude distributions over the plane and zero phase error from plane phase.

2. Practically speaking, if the maximum transmission path is to be realized with low loss, propagation must be predominantly in the lowest order beam mode (refs. 16 and 17), which is one with maximum amplitude in the center, tapering monotonically toward zero at the edges of the beam.

3. Requirement 2 indicates the desirability of use of a dominant mode waveguide terminating in a simple horn, which would radiate a spherical wave concentrated along the axis of the waveguide, and either a lens or parabolic reflector to correct the wavefront from spherical to plane. Requirement 1 translates into requirements that the waveguide horn have a well defined center of phase as a function of radiation angle, and that the center of phase in E and H planes be coincident. Further, it is necessary that the center of phase be invariant with changes in frequency over the approximately 2:1 waveguide band.

4. Finally, the horn must be simple in construction so that it can be fabricated at any wavelength for which dominant mode rectangular waveguide is feasible, even in very short lengths.

Open ended waveguide or waveguide with only very slight flaring to form a horn is suitable for feeding paraboloids or deeply curved meniscus lenses having short focal lengths or low f-number of the order of f:0.25. However, a large reflector with a focal ratio this small is impractical at short wavelengths because one cannot tolerate the loss in waveguide from the terminal device (detector or source) at the reflector edge out of the beam in to the focal point, nor can one tolerate the aperture blocking suffered when a relatively bulky device is placed in the center of the reflector in order to minimize waveguide length. Short focal length lenses require large amounts of dielectric material, and because of the relatively high losses of dielectric transmission at short wavelengths, they have not been considered practical. If one can use a reflector with a focal ratio of at least f:1, it is possible to keep the waveguide run from the device to the feed horn short so that losses are small, and yet keep the terminal devices out of the plane wave in the aperture of the paraboloid. This is done by feeding the paraboloid through a small hole in a 45° flat reflecting mirror as shown in figure 1. Thus the remaining problem of consequence in realizing satisfactory terminal optics is the design of a simple effective feed horn for an f:1 paraboloid.

High quality feed horns for such comparatively long focal length

systems have been designed (refs. 18 and 19) which maintain good control over unwanted sidelobe radiation. Neither of the designs referred to are suitable for the present application, however, because they appear to be fairly narrow band in performance, and they are certainly much too complicated to fabricate at wavelengths of a few tenths of a millimeter where it should be feasible to fabricate and use short sections of waveguide.

A waveguide feed horn which does a fair job of satisfying the above requirements is shown in figure 6. This horn is dimensioned for RG-98/U waveguide. Because no equipment was available for testing such a device in the region the spectrometer is used, development was performed at X-band and the dimensions scaled. Figure 7 outlines the performance of the crossed-pyramid horn. It can be seen that the amplitude distribution is the same for E-plane, H-plane and 45° cuts, and that the phase center is essentially constant over a wide angle and is at the same point in both E and H planes. This horn, on which the greatest amount of data was taken, is suitable for use with an f:0.75 reflector. A modified design was used with the f:1 spectrometer optics. This design was taken from the data in figure 8, which graphs the axial length and included angle of horns as a function of their beamwidth at 3, 10, and 20 db below the peak.

It is felt that the horn design shown in figure 6 can be fabricated down to extremely short wavelengths. It is probable that conventional machining techniques may be used down to wavelengths of the order of 1 mm where waveguide dimensions are of the order of 0.45 x 0.9 mm (0.0175 x 0.035 inch). At shorter wavelengths the following procedure would be used. A pyramidal hob would be ground in a suitable hard material. This hob would be forced into the material from which the horn is to be made, leaving a pyramidal depression. Two of these depressions should be made, each in a separate block. In a milling operation, followed by lapping, one side of each depression is milled away along a diagonal leaving only half of each pyramid. In the milled side of each block along the axis of the horn a square groove is cut which is one half of the rectangular waveguide. This operation would be performed with a single-toothed slitting saw in the manner used successfully by CSF in the fabrication of Carcinotron structures (ref. 20). The two blocks are then pinned or sweated together and the face of the horn milled and lapped to give the correct horn length. A short focal-depth microscope on a three-dimensional calibrated traverse will be indispensable for gauging the horn at various stages of the above process.

III. INSTRUMENTAL CHARACTERISTICS

Data Recording and Processing

There are several notable differences in the procedure of using an interference spectrometer compared to conventional grating or prism spectrometers. In the latter case, spectral information is obtained directly in the detector output as a function of the grating scan angle, whereas in the former case the interferogram must be processed in order to obtain spectral data. In addition, useful information is contained in the interferogram for long path delays at which the apparent signal-to-noise ratio is zero as judged from an analog plot. The availability of a digital computer for performing the necessary fourier transformation of the interferogram makes it highly desirable to record the interferogram directly in digital form; the large amount of data required to realize the maximum resolution makes the use of digital recording and handling techniques mandatory.

The spectrometer output and recording arrangement which is presently used is shown in figures 9 and 10. The output of the phase sensitive detector is digitized by a voltage-to-frequency converter whose output is counted for one second on command from a set of cam-driven contacts on the interferometer screw drive. The counter decades are read with a Dymec scanner for punching. The final output medium is serial paper tape in a BCD form compatible with the available Burroughs 220 computer. The phase-sensitive amplifier contains controls for adjusting gain and offset levels of the output.

The details of calculation of the spectral power density function from the interferogram will not be described here. A very complete and sophisticated handbook exists written by Mme. Janine Connes (ref. 12). However, several aspects of the process of obtaining the spectral power density function need to be discussed in order to interpret results which characterize the performance of this spectrometer.

Resolution. Whereas ideally the spectrum, $B(\nu)$, should be calculated from

$$B(\nu) = \int_{-\infty}^{\infty} V(x) \cos(2\pi x\nu/c)\, dx \quad , \tag{9}$$

a transformation of an interferogram over an infinite range of path delay, x, in practice the integration which is performed is

$$B(\nu) = \int_0^L V(x)\, A(x)\, \cos(2\pi x\nu/c)\, dx \quad . \tag{10}$$

This transformation differs from (9) in that the integration is performed over a finite range of delay, $0 \leq x \leq L$, and an apodizing function, $A(x)$, has been included. Integration from the center out to $x = L$ is allowed because of the symmetry of (9). The effect of terminating the integral at $x = L$ is to introduce a smearing of the spectral function. For example, if the original power spectrum were a monochromatic line at $\nu = \nu_o$, then $V(x)$ would have the form $V_o \cos(2\pi x\nu_o/c)$. This interferogram function calculated in (10) with $A(x) =$ constant would result in

$$B(\nu) \approx \frac{V_o L}{2} \sin[2\pi(\nu-\nu_o)L/c]/[2\pi(\nu-\nu_o)L/c] \quad . \tag{11}$$

This familiar function has a width at half height of only 0.6 c/L whereas it has undesirable "sidelobes" which are of the order of 25 per cent of the main peak. If one makes $A(x)$ an appropriate monotonic decreasing function of x, the sidelobe level can be substantially reduced.

The apparatus function of equation (11) has a peak amplitude which increases as L. If $B(\nu)$ is divided by $V_o L/2$, then the resulting function is a spectral power density referred to the bandwidth $\Delta\nu \approx c/L$.

The numerical integration which was performed by the digital computer is

$$B_n(\nu) = \frac{1}{2} V_M + \sum_{j=1}^{N} V_{M+j}\, A_j\, \cos(j2\pi\Delta x\nu/c) \tag{12}$$

where M is the index of the designated zero point and Δx is the differential path length change between data points. In all of the examples presented in this report the apodizing function $A_j = (1 - j\,N)$ was used, and no attempt was made to estimate and use an interferogram zero point lying part way between two data points. The above apodizing function gives a width of the spectral function at half height of about 0.9 c/L and has

sidelobes about 6 per cent of the peak.

Signal Power Density and Noise

At wavelengths and temperatures where the Rayleigh-Jeans approximation to the Planck law is valid, a matched (black) radiation source at temperature T_s will deliver in a bandwidth $\Delta\nu$ an amount of power

$$P_s = k\, T_s\, \Delta\nu \quad .$$

The signal-to-noise ratio for a detector with known NEP may be calculated from

$$S/N = \frac{k\, T_s\, \Delta\nu\, 0.5\, \Gamma}{NEP \sqrt{B_v}} \tag{13}$$

where B_v is the post-detection integration bandwidth and Γ is the transmission factor of the interferometer. The factor of 0.5 is included to account for that portion of the radio-frequency power which results in a dc bias in the interferogram.

Example

Assume an interferogram composed of 350 samples each one second long spaced 0.00833 inch apart in path delay. A noise source with T_s = 14,700 degK and detector with NEP = 6^{-11}* watt/cps$^{1/2}$ at the peak of its response are used. The processed spectrum will have a spectral resolution approximately given by $\Delta\nu \approx c/L = 3^{10}/(2.54 \times 350 \times 0.00833) = 4$ gc. The integration bandwidth is $B_v = 1/(2\pi \times 350) = 4.5^{-4}$ cps. Thus for these parameters and an interferometer transmission Γ of 0.4 (4 db loss), one should expect a signal-to-noise ratio of

---

*In this notation numbers between 1 and 10 which are followed by a superscript are multiplied by 10 raised to the superscript power. Thus 6^{-11} implies 6×10^{-11}.

$$S/N = \frac{1.38^{-23}\ 1.47^{4}\ 4^{9}\ 0.5\ 0.4}{6^{-11}\ 2.2^{-2}\ 10}$$

$$= 123$$

at the peak of the detector response.

In figure 11 are shown spectrum calculations of three independent interferograms taken for the same spectrometer conditions; that is, the only difference between the interferograms, and hence between the spectra, should be caused by the noise of the detector. From figure 11 the rms noise is estimated to be 0.8 power units while the maximum displacement is of the order of 18.5 power units; these result in a signal-to-noise ratio of 23.

In comparing this ratio with the result of the previous calculation, a discrepancy of a factor of 5 is noted. This is partly due to the fact that in the calculation the modulation efficiency was not considered, nor was the effect of apodization on the signal-to-noise ratio. Together these account for a factor of 2, leaving a discrepancy of a factor of 2.5 unexplained.

The noise equivalent power of a detector may be estimated using equation (13) and an additional bit of information: that the audio signal-to-noise ratio of the detector is 20 db when the interferometer is set at its zero point (equal path lengths in the two arms). In this measurement the amplifier bandwidth was 5 cps, and the source temperature is assumed to be 1.47^{4} degK. From figure 11 the effective detector bandwidth is estimated to be 18 gc. The noise equivalent power of the detector may be calculated from

$$NEP = \frac{k\ T_s\ B\ \Gamma}{\sqrt{B_v}\ S/N}$$

$$= \frac{1.38^{-23}\ 1.47^{4}\ 1.8^{10}\ 0.4}{2.24\ 10}$$

$$= 6.5^{-11}\ \text{watts/cps}^{1/2}$$

This is in accordance with the determination of Long and Butterworth (ref. 21) made with another instrument.

Spectral Bandpass

The background shape of a spectrum obtained with the spectrometer such as the one shown in figure 11 is determined by a number of factors. The most obvious and influential factor in this case is the response of the bolometer detector. The bolometer is an evacuated waveguide barretter* which is apparently tuned for maximum response at 50 gc. The effective temperature and emissivity of the noise source also affect the shape of the spectrum. The noise source used in the tests of the instrument was a waveguide mounted low-pressure neon plasma** with an advertised effective temperature in the RG-98/U waveguide band of 14,700 degK. The failure of its output at wavelengths shorter than about 4 mm probably contributes to the apparent lack of radiation at short wavelengths.

An important influence on the spectral shape is the depth to which various spectral components are modulated by the interferometer. As was emphasized in chapter I, only energy propagating through the interferometer in the lowest order plane wave alone is fully modulated. Thus energy at high frequencies at which the horn feeds launch many modes may not be modulated. One is lead to the concept of a modulation efficiency, the fraction of total energy which is ideally modulated by the interferometer. Spot checks at several frequencies in the range of 63 to 73 gc with a c-w source indicated modulation efficiencies of 0.95 to 0.98. However, reference to figure 12, which is a plot of part of an interferogram taken with the broadband noise source, indicates a net modulation efficiency of only 0.70. This reduction in efficiency is believed to be caused by energy at high frequencies not being modulated and perhaps by slight misalignment of the waveguide horns, which allows more energy to propagate in one side of the interferometer than in the other.

An extreme example of reduction in modulation efficiency is afforded by the result of an experiment in which a high pressure mercury arc was used as a noise source without a waveguide feed. While the total power received by the bolometer was large, it was radiated from the extended area source and propagated through the interferometer in many modes. Thus it was not surprising to observe a modulation efficiency of only 0.10 in this case.

---

*PRD Electronics holder type 634 with PRD type 632 and MSI Electronics type 134 barretters.

**Roger White Electron Devices type GNW-18-V.

The same mercury source was used with a waveguide horn feed in order to select a single mode. Although the total power at the zero point was reduced drastically, the modulation efficiency was then high. The spectra calculated for both these cases are plotted over each other in figure 14 and indicate that the modulated power received was the same in each case. The signal-to-noise ratio is small here because this source, a 250 watt mercury-arc street lamp, has a low effective temperature (estimated to be about 1300 degK).

Effect of Choice of Zero Point

There are two primary effects of variation of choice of the zero point of the interferogram: asymmetry of the spectral function and a periodic baseline shift. These are illustrated in two tests which were attempted to display the characteristics of the spectrometer. In one the input of the spectrometer was a monochromatic wave obtained from a klystron and frequency multiplier. The spectra which were calculated are shown in figure 13. Calculations were made using three different length sections of the interferogram corresponding to maximum path delay lengths of 18.3, 38.5 and 81 cm. The widths at half height of the peaks are 1550, 720 and 330 mc, respectively. In these calculations a triangle function was used for apodization, and the same zero point for the interferogram was used in each. Note that the sidelobe structure is not symmetric, which indicates that the choice made of zero point was not precise and that it differed from the correct one by about 0.15λ (refs. 12 and 22). No attempt was made to recalculate this spectrum using a better estimate of the zero point.

In figure 15 are shown transmission curves of a high-pass filter. This filter was made by introducing a section of rectangular waveguide with reduced H-plane dimension in front of the detector. This choke section will not propagate energy with wavelength greater than twice the width of the waveguide. Two calculations are shown with the filter using triangular apodization and sections of the interferogram 11.5 and 41.5 cm long resulting in spectral resolutions of about 3 and 1 gc, respectively. The dotted curve bounds the spectrum power which was blocked by the filter.

Several comments are appropriate to the curves of figure 15. The cut-off slope of the filter is much sharper than that revealed by these calculated spectra; that is, the slope is limited by the interferogram length used rather than by the filter characteristic. The oscillation in the 1 gc resolution curve is very much greater than that of the 4 gc resolution curve. This cannot be explained as an increase in the spectrum noise caused by using a longer section of interferogram because a length increase of four times should increase the noise fluctuation only by a factor of two. The fluctuation might be produced by multiple reflections between the detector, the filter section and the receiver waveguide horn, all of which have about the correct separation to give the observed

periodicity. However, this would not account for the fluctuation in the stop-band region where tunnelling through the filter is certainly negligible. The rapid growth of amplitude of the fluctuations with decreasing spectral resolution suggests a transient phenomenon associated with the sharp discontinuity of the spectrum, but the exact nature has not been determined.

The effect of variation of choice of the zero point for the interferogram on shifting the baseline of the spectrum is illustrated in figure 16 using the same data sample as curve B of figure 15. The three curves of figure 16 represent choices of zero point differing by about $\lambda/30$ at 50 gc. Qualitatively they are similar but there are major differences in the indicated spectrum level. The discrepancy is most obvious at frequencies below 50 gc, where there is certainly no energy reaching the detector.

The problem of locating the correct zero point is presently the most vexing in the use of the spectrometer. Mechanical methods are inadequate because different setups and adjustment conditions of the interferometer will vary the point of zero differential path delay. The little experience gained with the instrument has indicated that recalculation of an interferogram with new trial selections for the zero point is the most successful way of finding the correct point. This redundancy of calculation is not entirely wasteful, however, because if different interferograms are used in which the detector noise is independent but all other conditions including the relationship of the data sampling control pulse to the drive screw remain unchanged, then the additional calculations also serve to define accurately the noise level in the spectrum. This was illustrated in figures 11 and 14.

IV. REVIEW

The principles of operation and construction of the interference spectrometer have been reviewed in order to reveal the peculiarities of use and the limitations of its applications to spectrometric problems. It is evidently an instrument peculiarly well suited to the long wavelength end of the difficult-to-instrument submillimeter region; in this region it will produce unusually small spectral resolution, 0.01 cm^{-1} or one part in 500, whichever is the greater limitation.

Problems in the development of the instrument were outlined, some of which resulted in unusual solutions. Notable are a method of fabricating at low unit cost parabolic reflectors of moderate size and accuracy and a moderately efficient waveguide feedhorn whose construction is so simple that fabrication is promised down to wavelengths where waveguide techniques are generally considered too difficult today.

The spectrometer in its present state is only partially completed, with compromises in the following areas. The mirror drive, a recirculating ball lead screw, has a relative accuracy of only about one part in 2000, which limits the spectral resolution to about one part in 500. Very few spectroscopic problems would be expected to require better resolution in this region. The small prolate spheroid reflectors have errors in figure which limit their usefulness to wavelengths longer than about 1 mm. The 12 inch diameter paraboloids are known to be accurate to $\pm 12\mu$ and may be better; therefore, they will certainly not limit operation at wavelengths longer than about 0.5 cm. The waveguide feed horns necessary to ensure single-mode plane wave propagation in the interferometer have been fabricated only for the 3.75 to 7.5 mm region. Other horn pairs will be required for operation at shorter wavelengths with this instrument. The only detector on hand for use with the instrument is a waveguide-mounted evacuated barretter bolometer which has useful sensitivity only in the region of 4 to 7 mm.

Only limited evaluation of the instrument has been made. Test results have been shown of a spectral "line" simulated by a klystron harmonic multiplier with a spectral resolution of 0.011 cm^{-1} (330 mc) and a high-pass filter transmission curve rising from negligible to full transmission in about 0.03 cm^{-1}. This latter spectrum shows features which are evidently a result of the fourier transformation process and are presently unexplained.

Georgia Institute of Technology,
Atlanta, Georgia, 8 May 1964.

REFERENCES

1. Long, M. W., and Rivers, W. K., Jr.: Submillimeter Wave Radiometry. Proc. Inst. Radio Engrs., vol. 49, 1961, p. 1024.

2. Ginsburg, N.: Research Concerning Far-Infrared Region of the Spectrum. Final Rep., Cont. AF 19(604)-2443, Syracuse University, 20 December 1961 (DDC AD 272 151).

3. Electronic Material Sciences Laboratory, Air Force Cambridge Research Center: Status Report, AFCRL 10, 3 January 1961, p. 92.

4. Yoshinaga, H., et al: Far Infrared Spectrograph for Use from the Prism Spectral Region to about 1 mm Wavelength. J. Opt. Soc. Am., vol. 48, 1958, p. 315.

5. Genzel, L., Happ, H., and Weber, R.: A Grating Spectrometer for the Region of the Far Infrared and Short Microwaves. Zeitschrift fur Physik, vol. 154, 1959, p. 1.

6. Strong, J., and Vanasse, G. A.: Lamellar Grating Far-Infrared Interferometer. J. Opt. Soc. Am., vol. 50, 1960, p. 113.

7. Genzel, L., and Weber, R.: Spectroscopy in the Far Infrared through Interference Modulation. Zeitschrift fur Angewandte Physik, vol. 10(4), 1958, p. 195. (Translation DDC AD 252 310).

8. LaFond, Charles D.: IR Spectrometer has Striking Sensitivity. Missiles and Rockets, 22 May 1961, p. 30.

9. Strong, J., and Vanasse, G. A.: Interferometric Spectroscopy in the Far Infrared. J. Opt. Soc. Am., vol. 49, 1959, p. 844.

10. Strong, J.: Concepts of Classical Optics, W. H. Freeman & Company, 1958.

11. Genzel, L.: Aperiodic and Periodic Interference Modulation for Spectrographic Purposes. J. Mol. Spectroscopy, vol. 4, 1960, p. 241.

12. Connes, J.: Spectroscopic Studies Using Fourier Transformations. Revue d'Optique, vol. 40, 1961, pp. 45, 116, 171, 231. (Translated as NAVWEPS Rpt. 8099, Naval Ordnance Test Station, China Lake, California. DDC AD 409 869).

13. Stroke, G. W.: Interferometric Method of Velocity of Light Measurement. Appl. Optics, vol. 2, 1963, p. 481.

14. Stewart, D. E.: Development of Lightweight Optically Accurate Replica Mirrors. Electro-Optical Systems Rpt. 2110-2Q-1, 15 June 1962 (DDC AD 277 372).

15. Noble, R. H., et al: Study and Analysis of Lightweight Optical Elements. Perkin-Elmer Corporation Rpt. 5857, October 1961 (DDC AD 271 408).

16. Goubau, G., and Schwering, F.: On the Guided Propagation of Electromagnetic Wave Beams. IRE Trans. Ant. & Prop., vol. AP-9, 1961, p. 248.

17. Christian, J. R. and Goubau, G.: Experimental Studies on a Beam Waveguide for Millimeter Waves, IRE Trans. Ant. & Prop., vol. AP-9, 1961, p. 256.

18. Potter, P. D.: A New Horn Antenna with Suppressed Sidelobes and Equal Beamwidths. Microwave J., vol. VI(6), 1963, p. 71.

19. Love, A. W.: The Diagonal Horn Antenna. Microwave J., vol. V(3), 1962, p. 117.

20. Convert, G.: A Backward-Wave Oscillator at 300 Gc. Millimeter and Submillimeter Conference, Orlando, Fla., 7-10 January 1963.

21. Long, M. W., and Butterworth, J.C.: New Technique for Microwave Radiometry. IEEE Trans. Microwave Theory & Tech., vol. MTT-11, 1963, p. 389.

22. Lowenstein, E. V.: On the Correction of Phase Errors in Interferograms. Appl. Optics, vol. 2, 1963, p. 491.

TABLE I.- IMPORTANT PARAMETERS OF MODEL INTERFEROMETER AND INTERFERENCE SPECTROMETER

Parameter	Model	Final
Test frequencies	15 gc	40-80 gc
Test wavelengths	2 cm	3.75-7.5 mm
Aperture size, D	61 cm, f:0.4	30.5 cm, f:1
D^2/λ	18.6 m	24.8-12.4 m
Path length in interferometer	2.75 m	2.1 m
Path length in units of D^2/λ	0.15	0.085 - 0.17
Transmission loss	3.7 db	4.0 db*

*Broadband loss. Includes source optics consisting of two prolate-spheroidal reflectors. Includes both diffraction losses and 0.5 db reflection loss due to mismatch at source and detector.

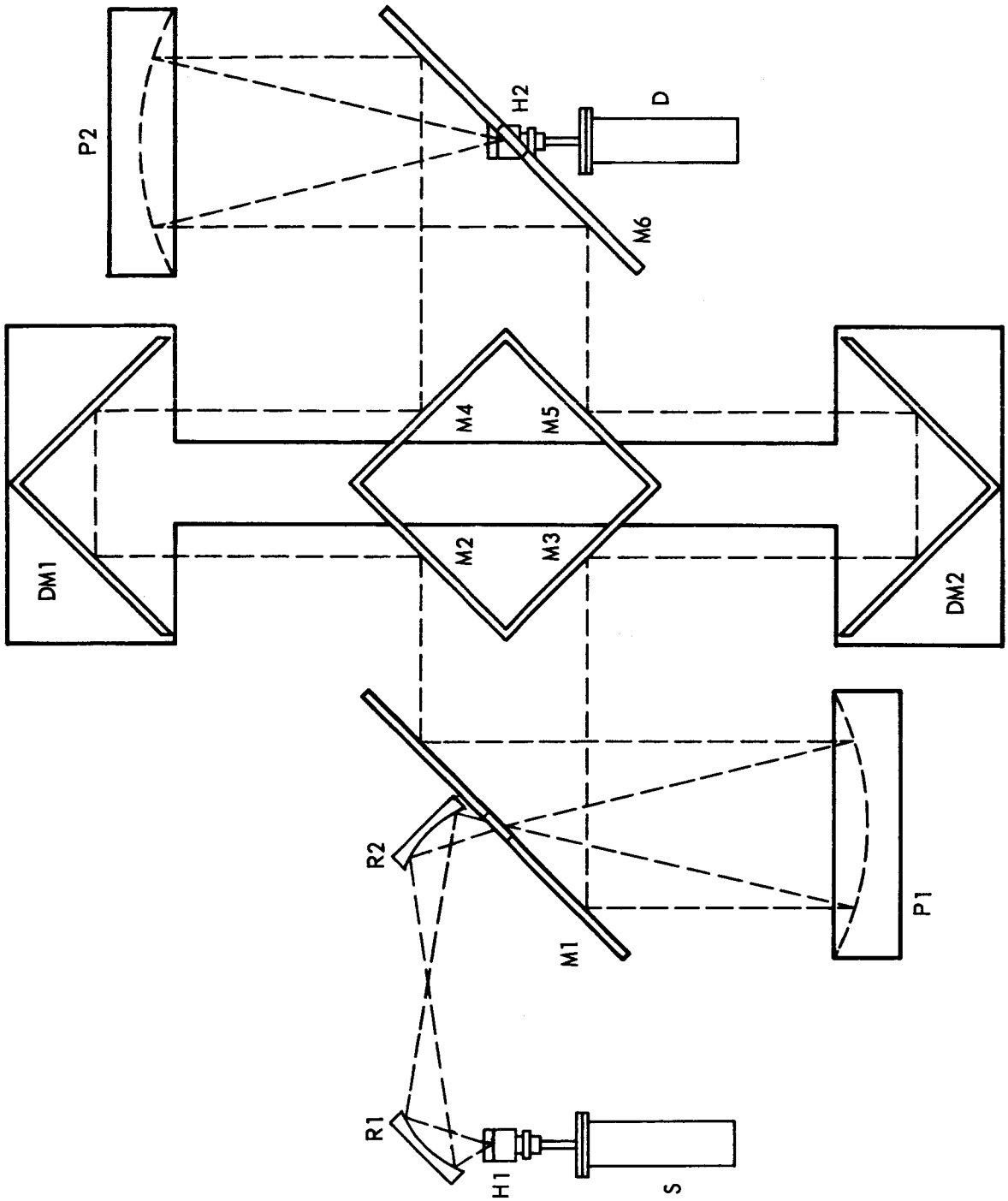

Figure 1. Schematic of Spectrometer.

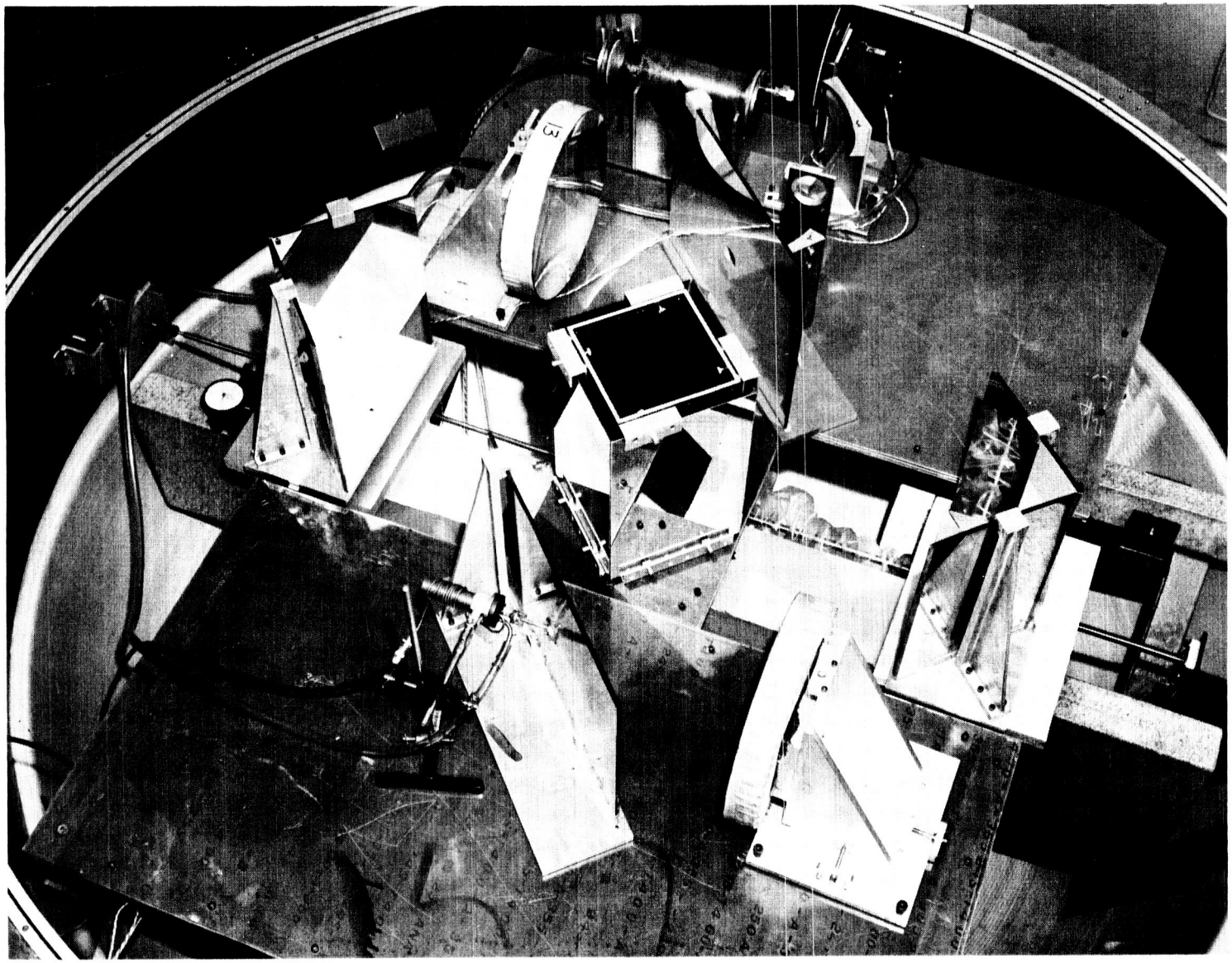

Figure 2. View of Spectrometer From Above. 40-80 gc Source, Detector and Waveguide Horns Installed.

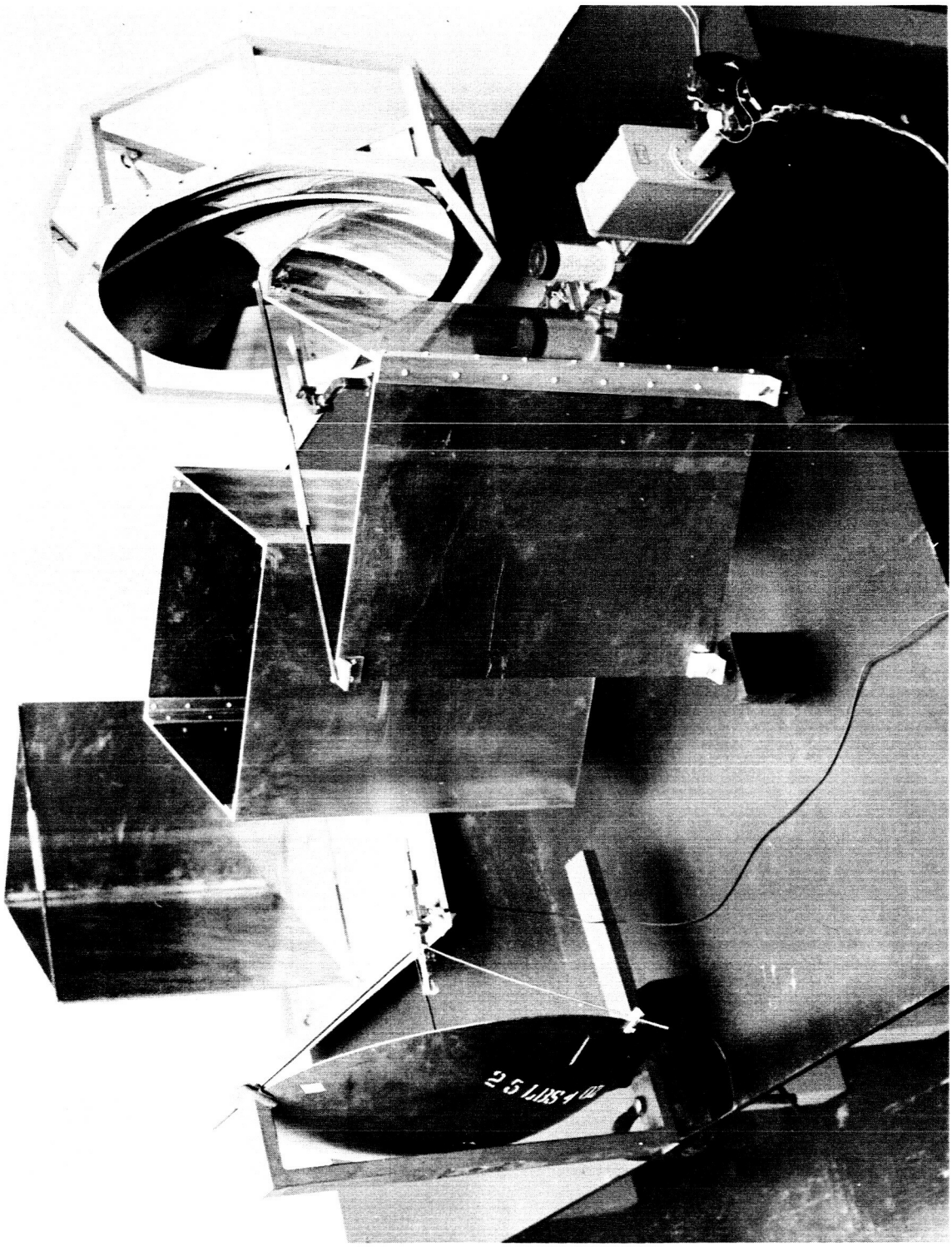

Figure 3. Model Interferometer.

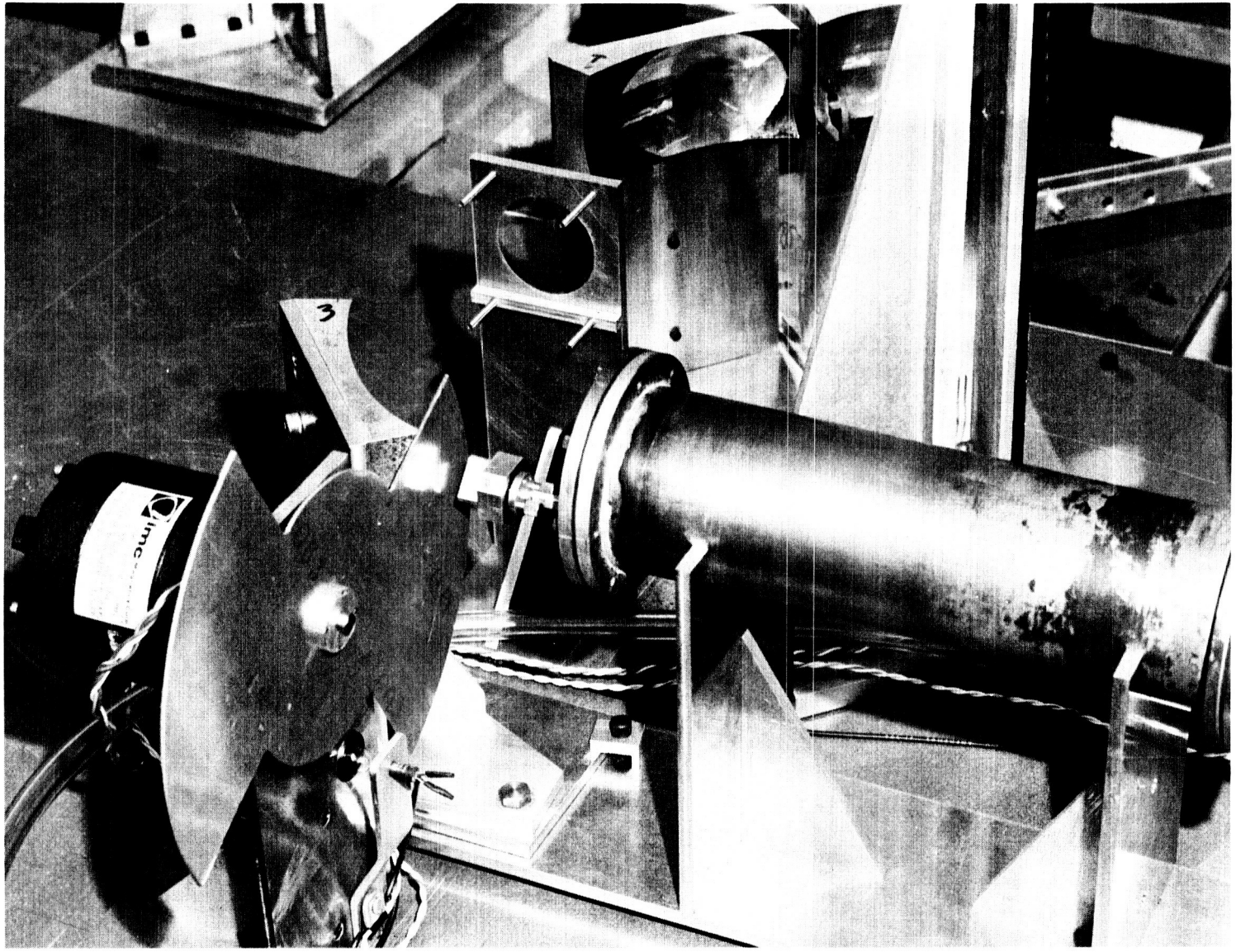

Figure 4. Source Optics of Spectrometer.

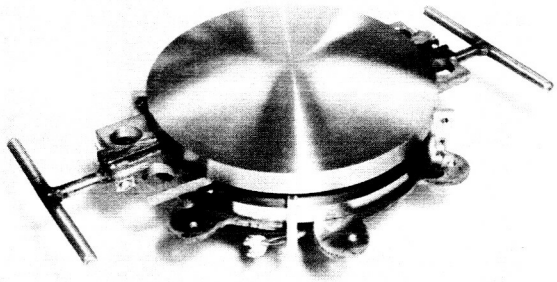

(A)

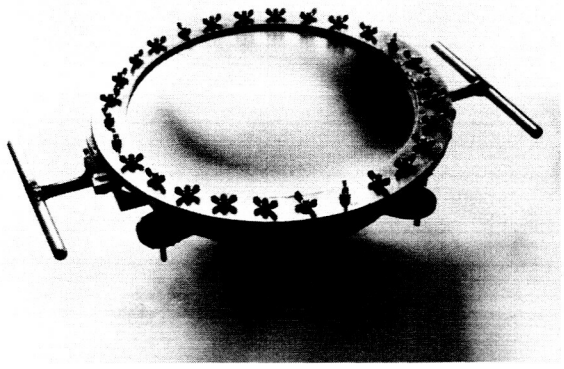

(B)

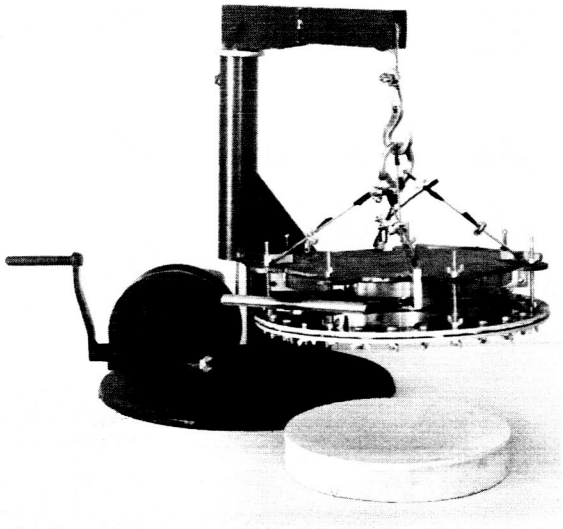

(C)

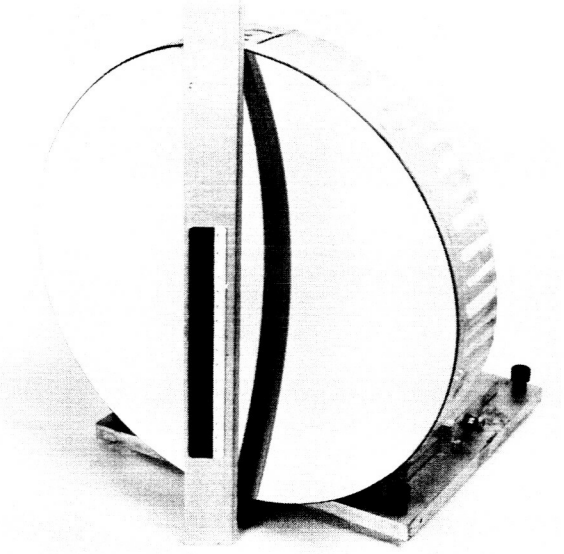

(D)

Figure 5. Construction of 12-Inch Parabolic Reflectors. (A) Stainless-Steel Male Mandrel. (B) Aluminum Foil on Frame Partially Stretched Over Mandrel. (C) Mandrel and Foil Inverted Over Fused-Silica Backing Structure Ready for Bonding. (D) Finished Reflector.

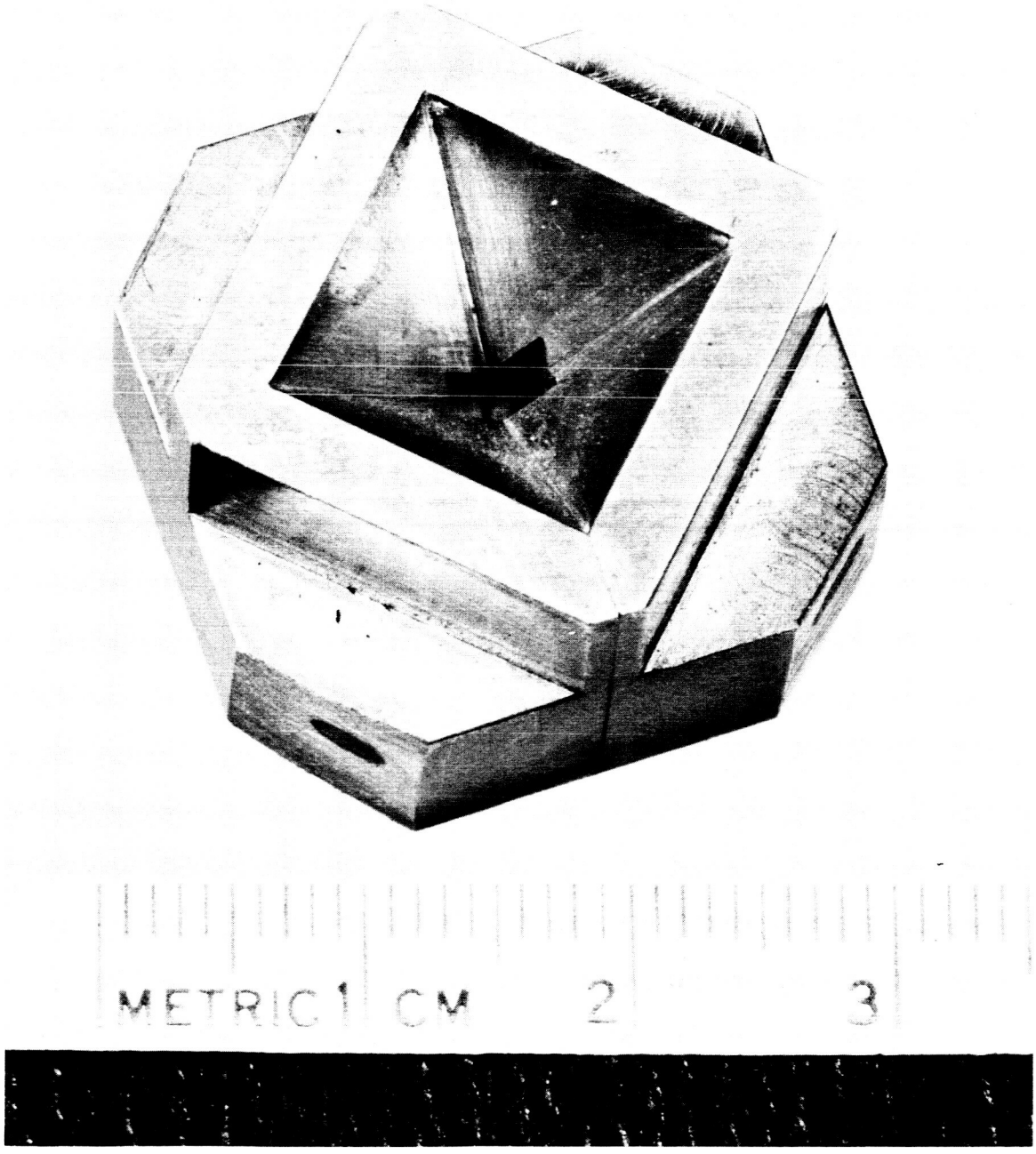

Figure 6. Machined Crossed-Pyramid Horn for 40-80 gc Region.

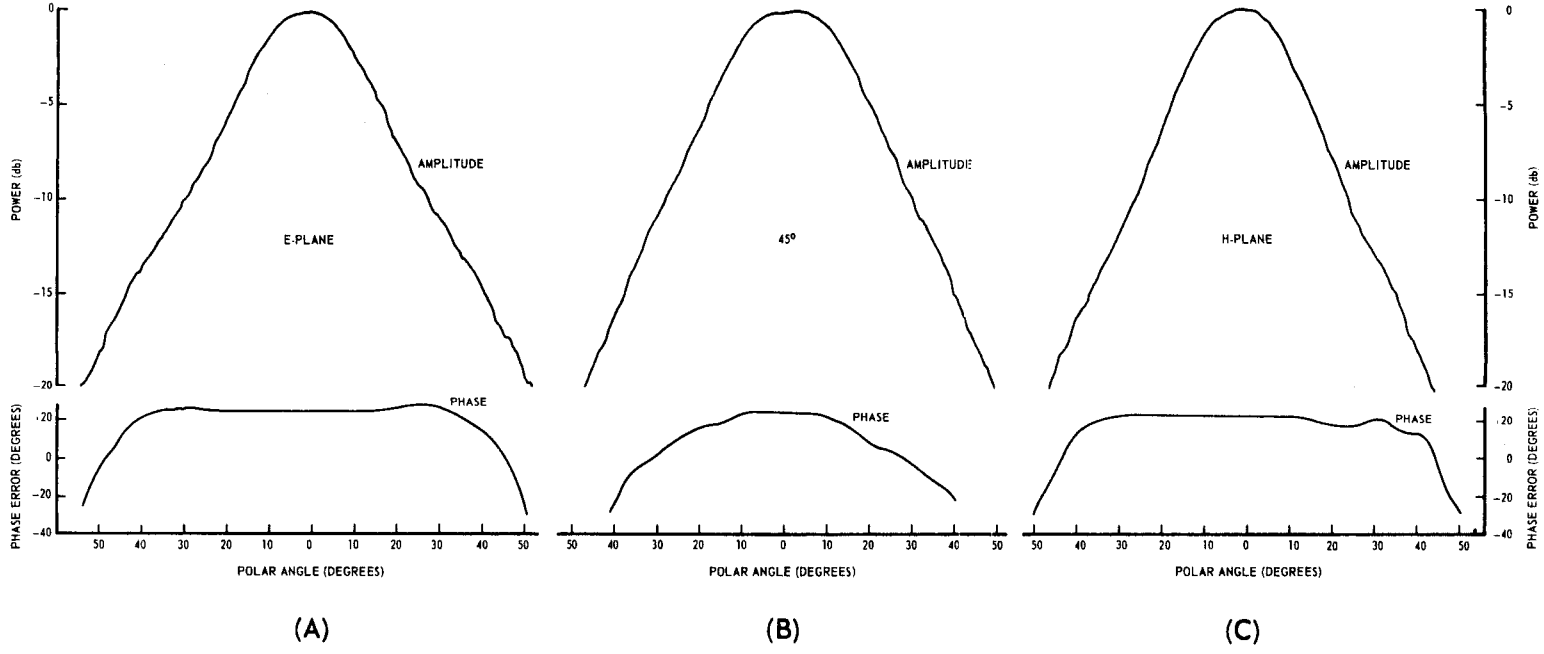

Figure 7. Amplitude and Phase Patterns of Crossed-Pyramid Horn. Patterns Taken on Developmental Model at 10 gc. Total Pyramid Angle Between sides 60°; Axial Length From Face to Apex 1.5λ. Phase Center at Apex of Pyramid. (A) E-Plane. (B) 45°. (C) H-Plane.

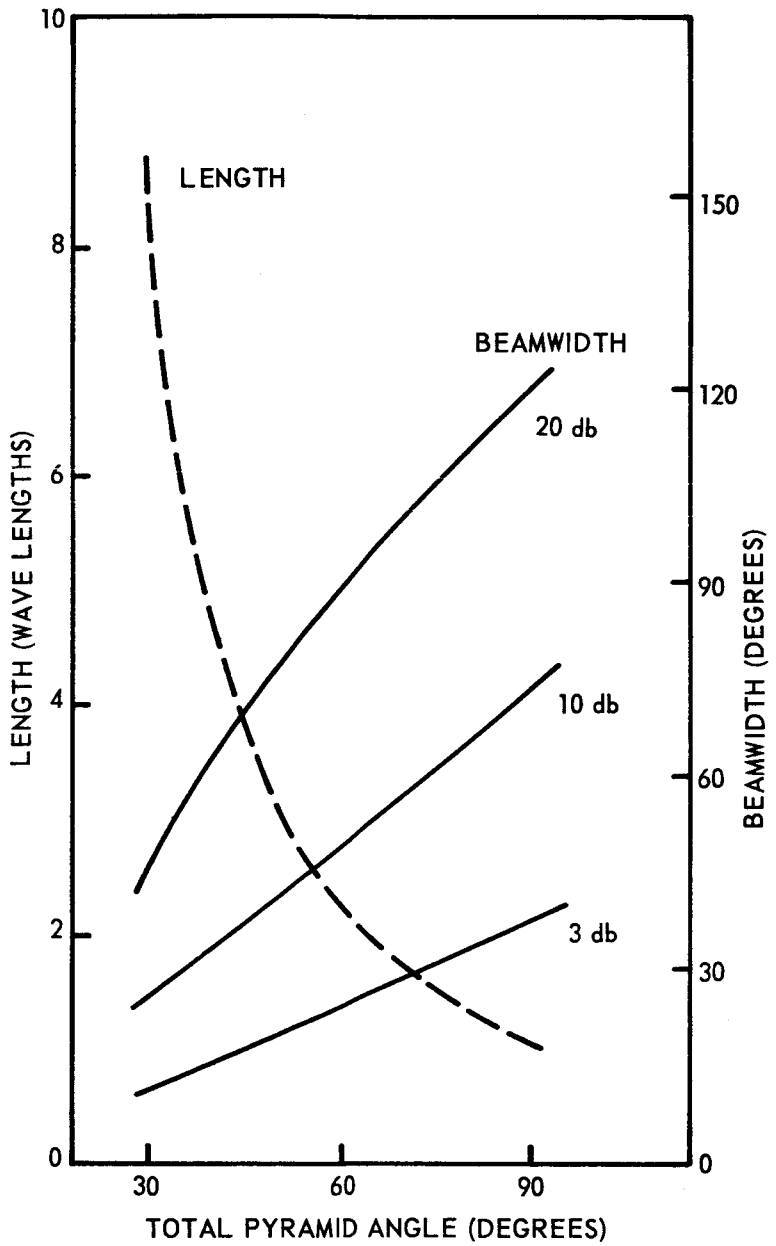

Figure 8. Beamwidths and Optimum Length of Crossed-Pyramid Horns. Length is From Face of Horn to Apex of Pyramid.

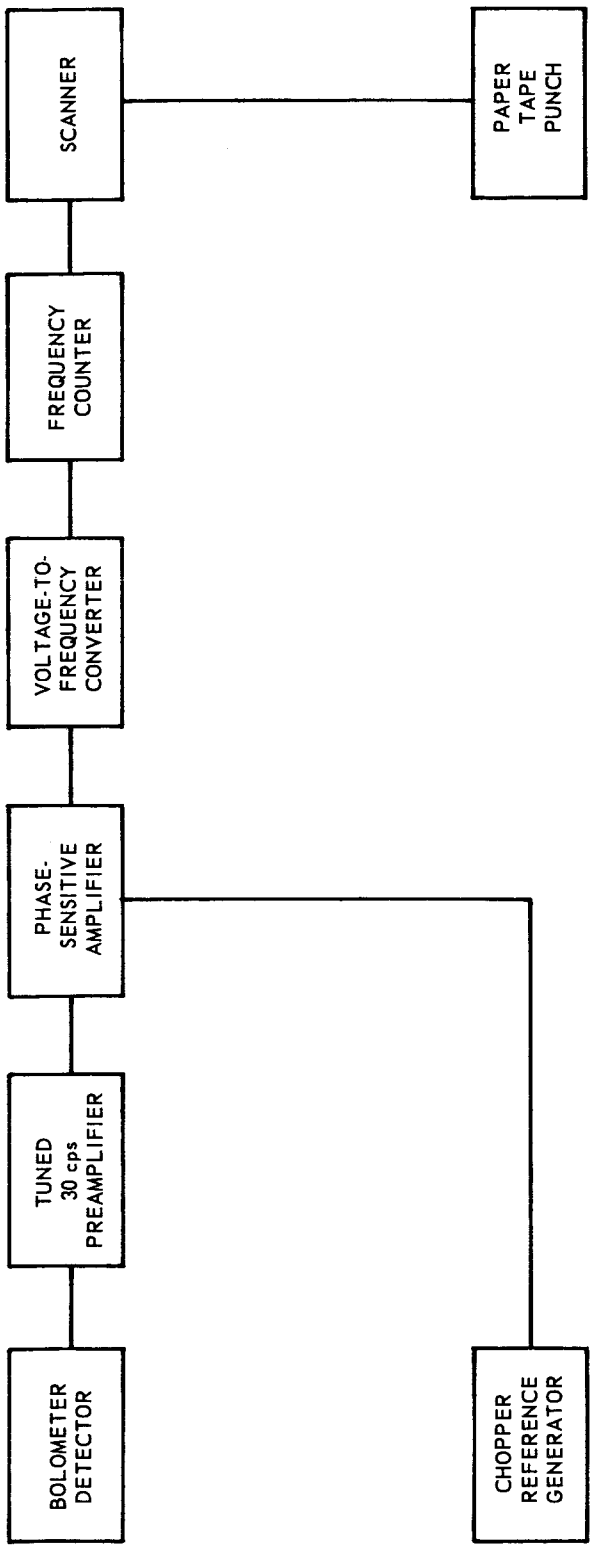

Figure 9. Block Diagram of Spectrometer Ouput and Data Recording Circuitry.

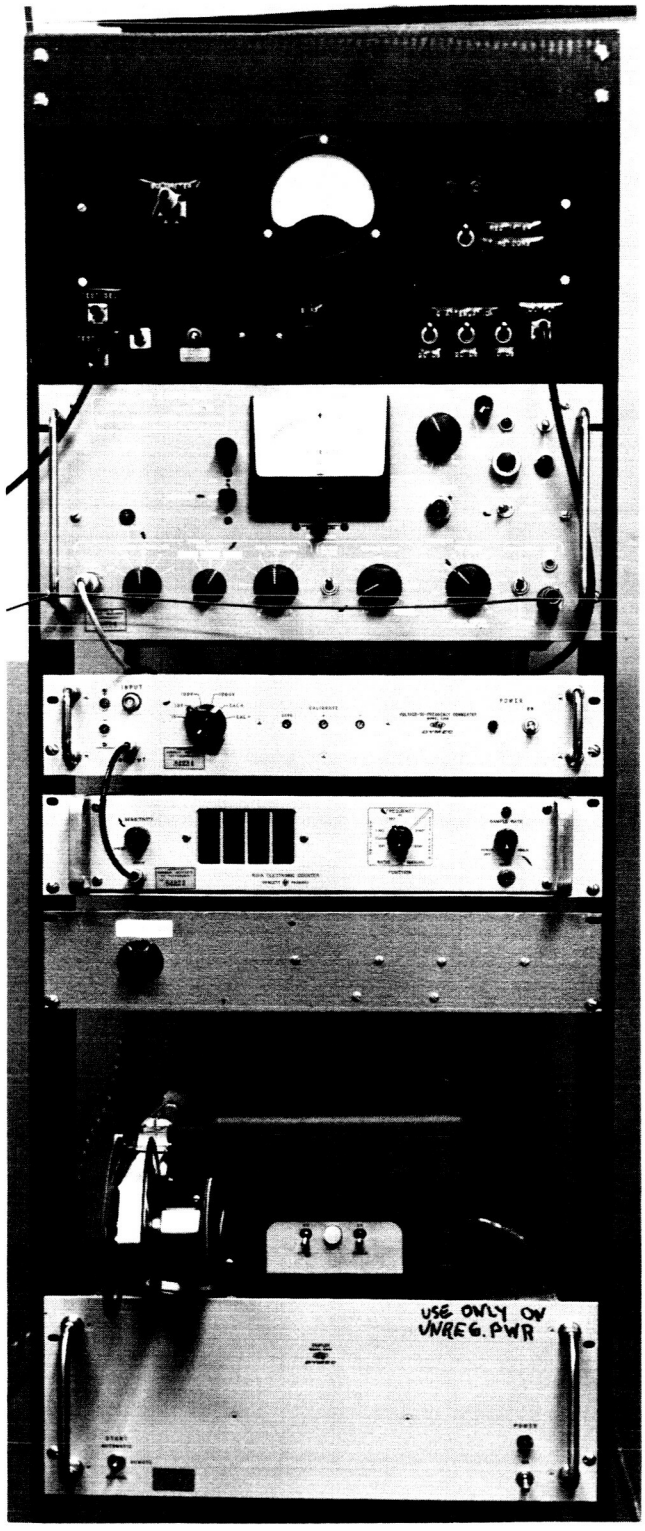

30-cps TUNED PREAMPLIFIER

PHASE-SENSITIVE DETECTOR

ELECTRONICS, MISSLES AND
COMMUNICATIONS, INC.
MODEL RJ-8

VOLTAGE-TO-FREQUENCY CONVERTER
DYMEC MODEL 2210

FREQUENCY COUNTER
HEWLETT PACKARD MODEL 5211A

CHOPPER CONTROL

PAPER TAPE PUNCH
FRIDEN MODEL SP-2

SCANNER-COUPLER
DYMEC MODEL 2540

Figure 10. Spectrometer Output and Data Recording Equipment.

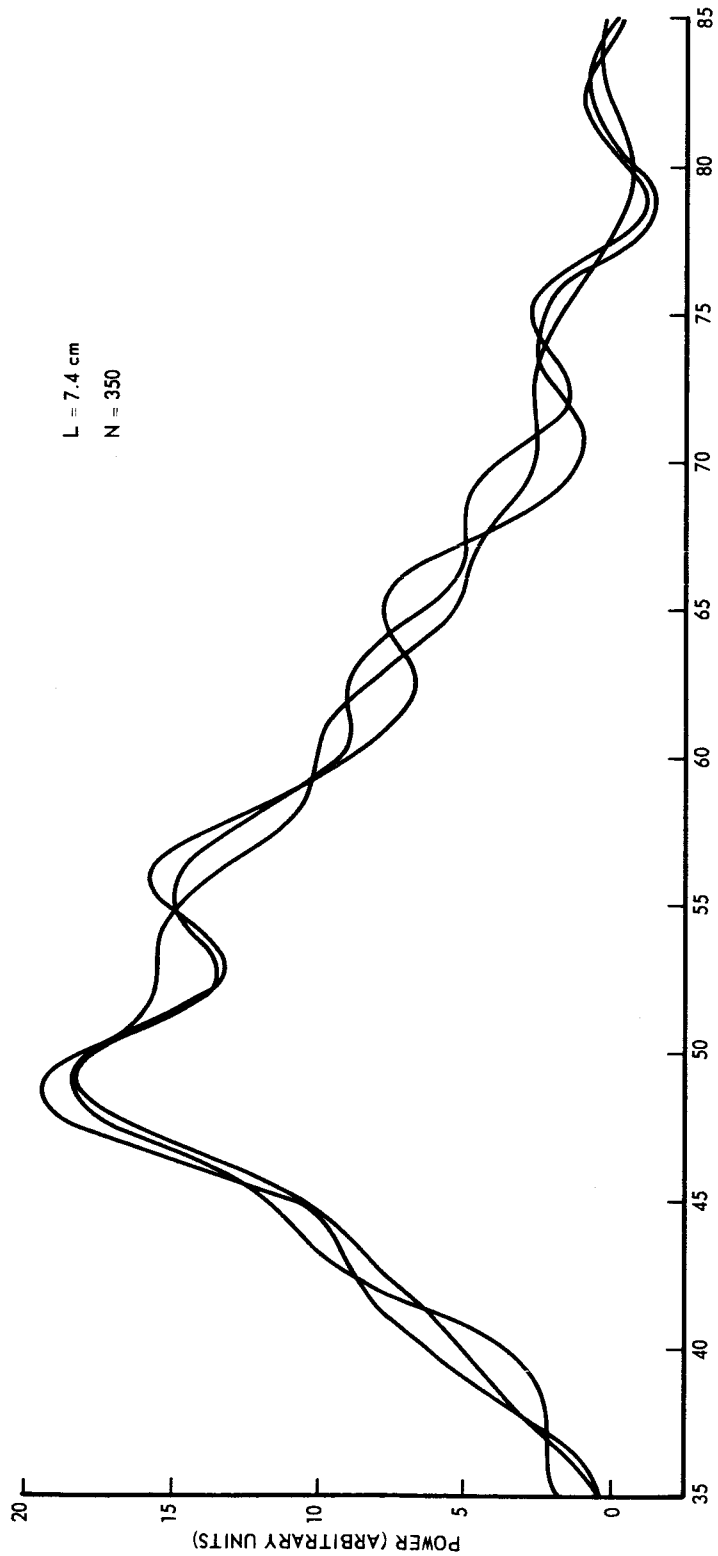

Figure 11. Bandpass of Spectrometer. Low Pressure Neon Noise Source and Evacuated Barretter Detector. Three Curves With Independent Detector Noise.

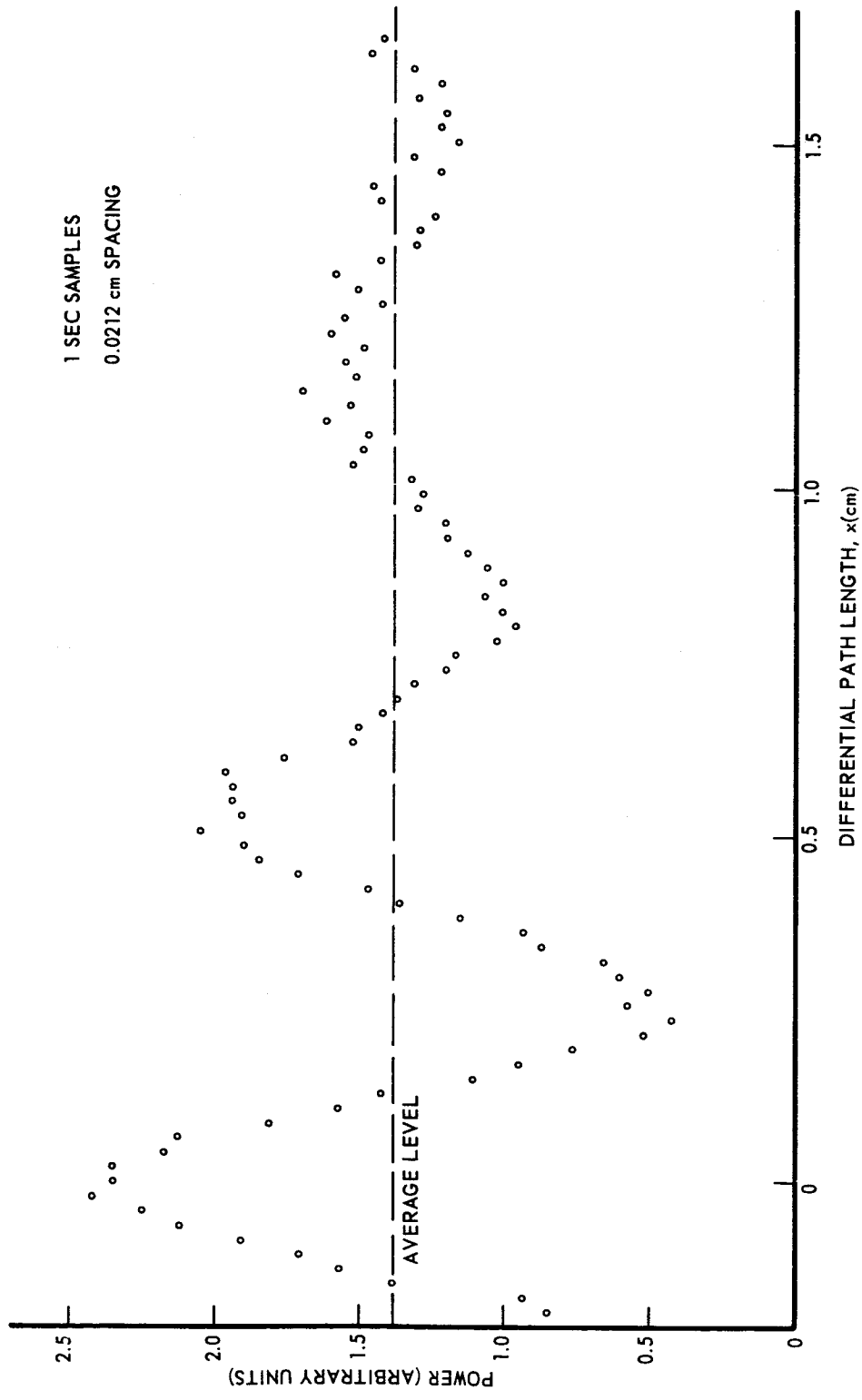

Figure 12. Portion of Interferogram.

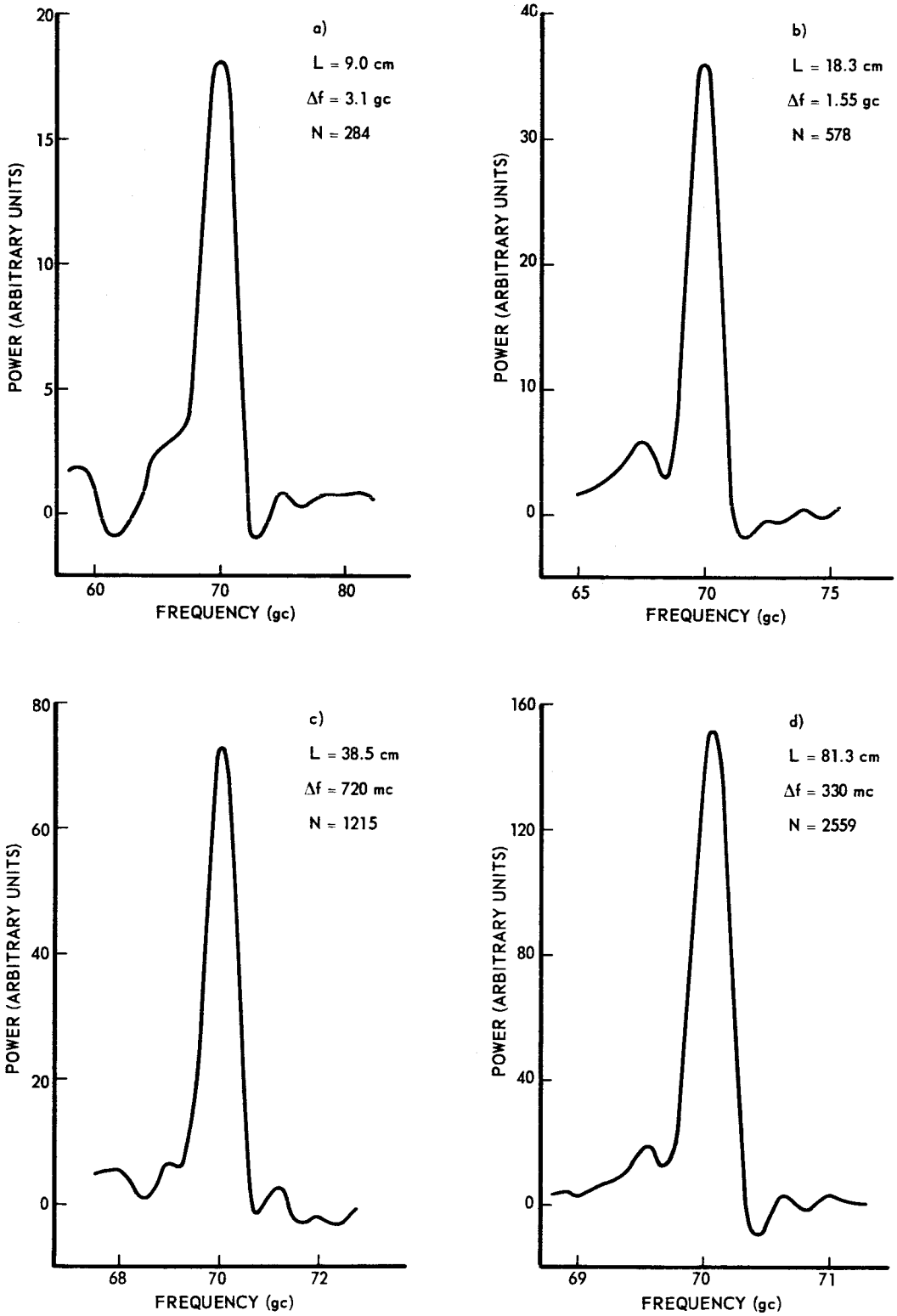

Figure 13. Spectra of Klystron Harmonic Multiplier. Each Spectrum Used Different Lengths of the Same Interferogram. Power Level $\sim 10^{-9}$ Watt.

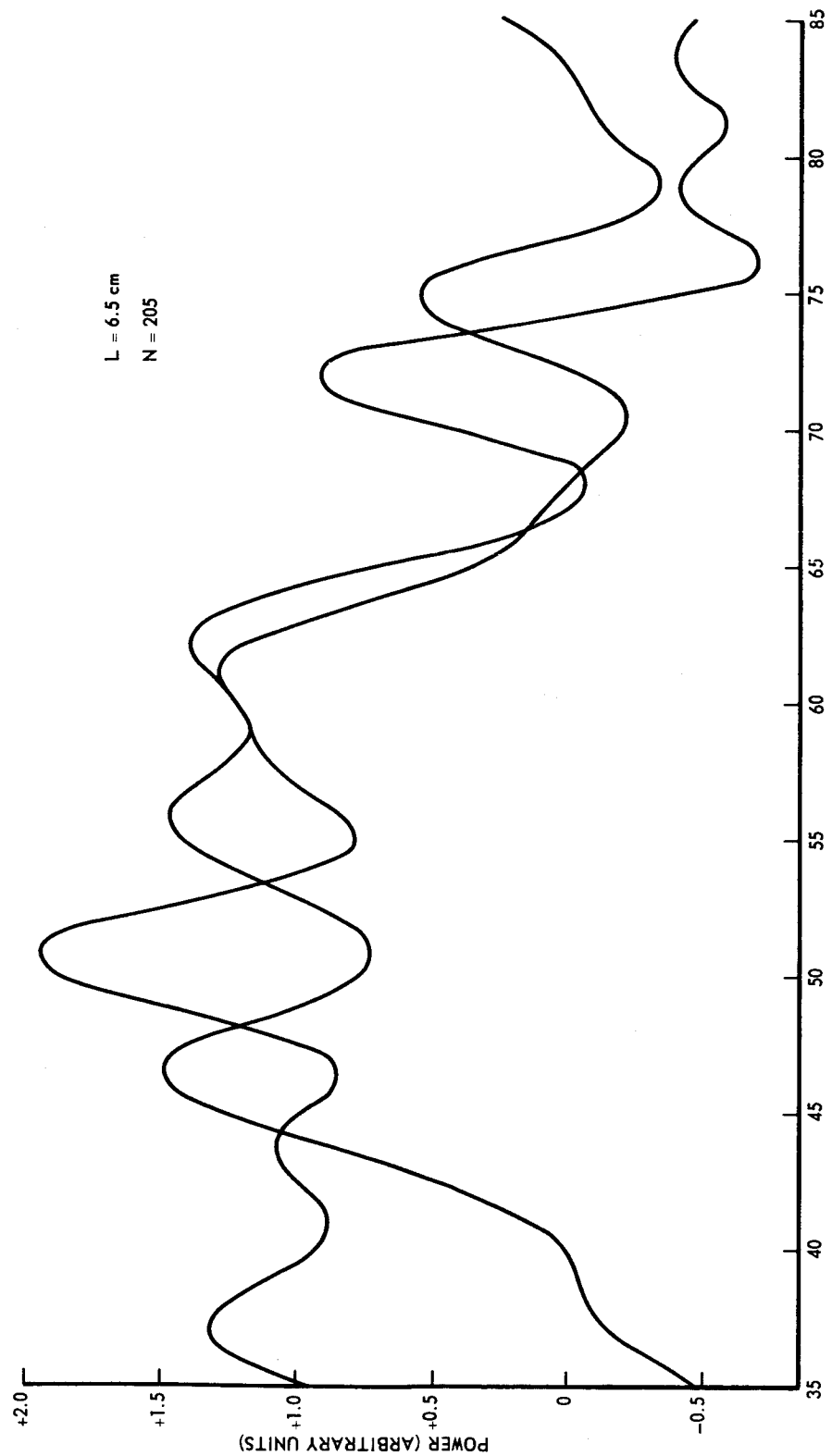

Figure 14. Spectra Using Mercury Arc and Evacuated Barretter Detector.

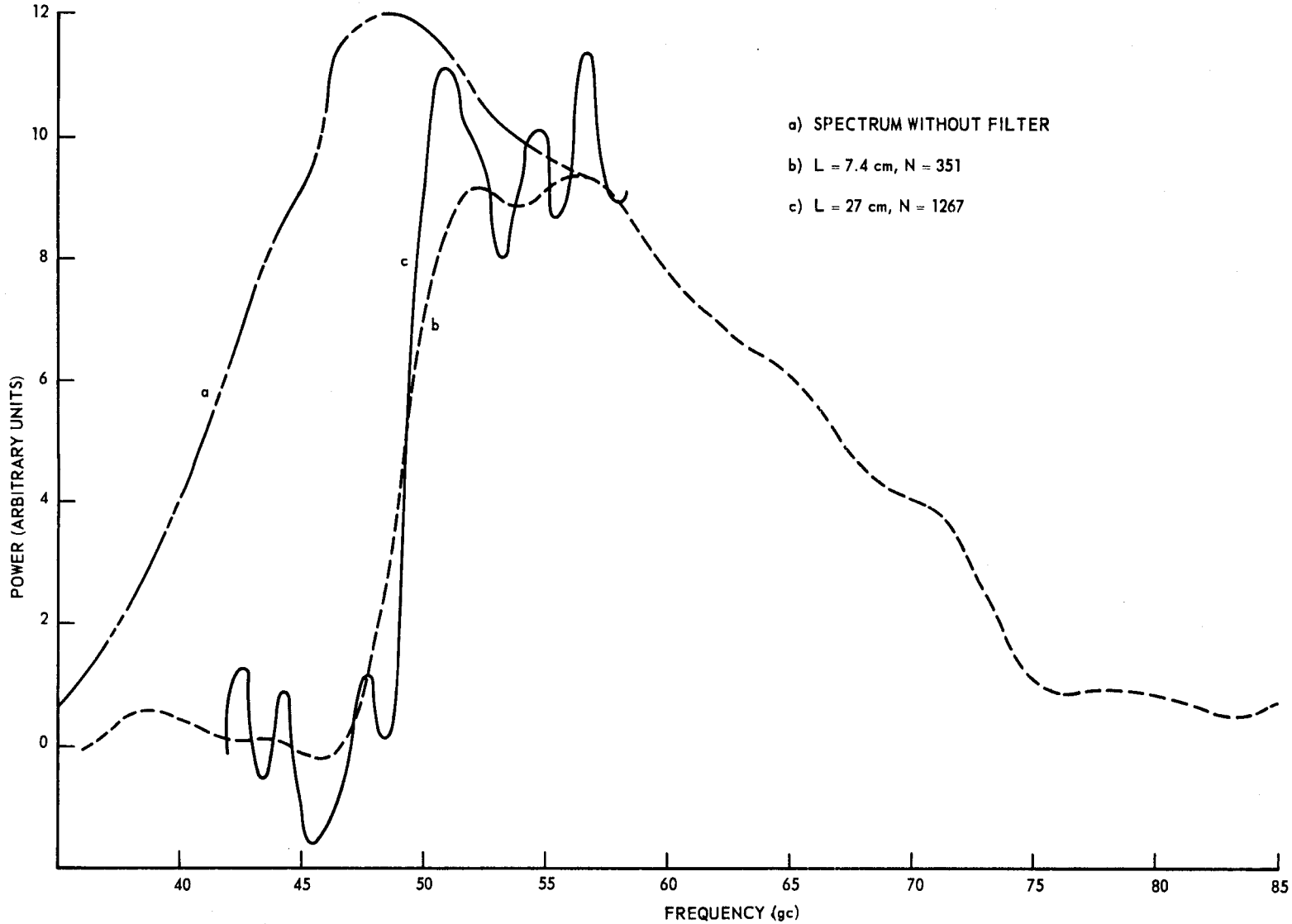

Figure 15. Transmission of a High-Pass Filter.

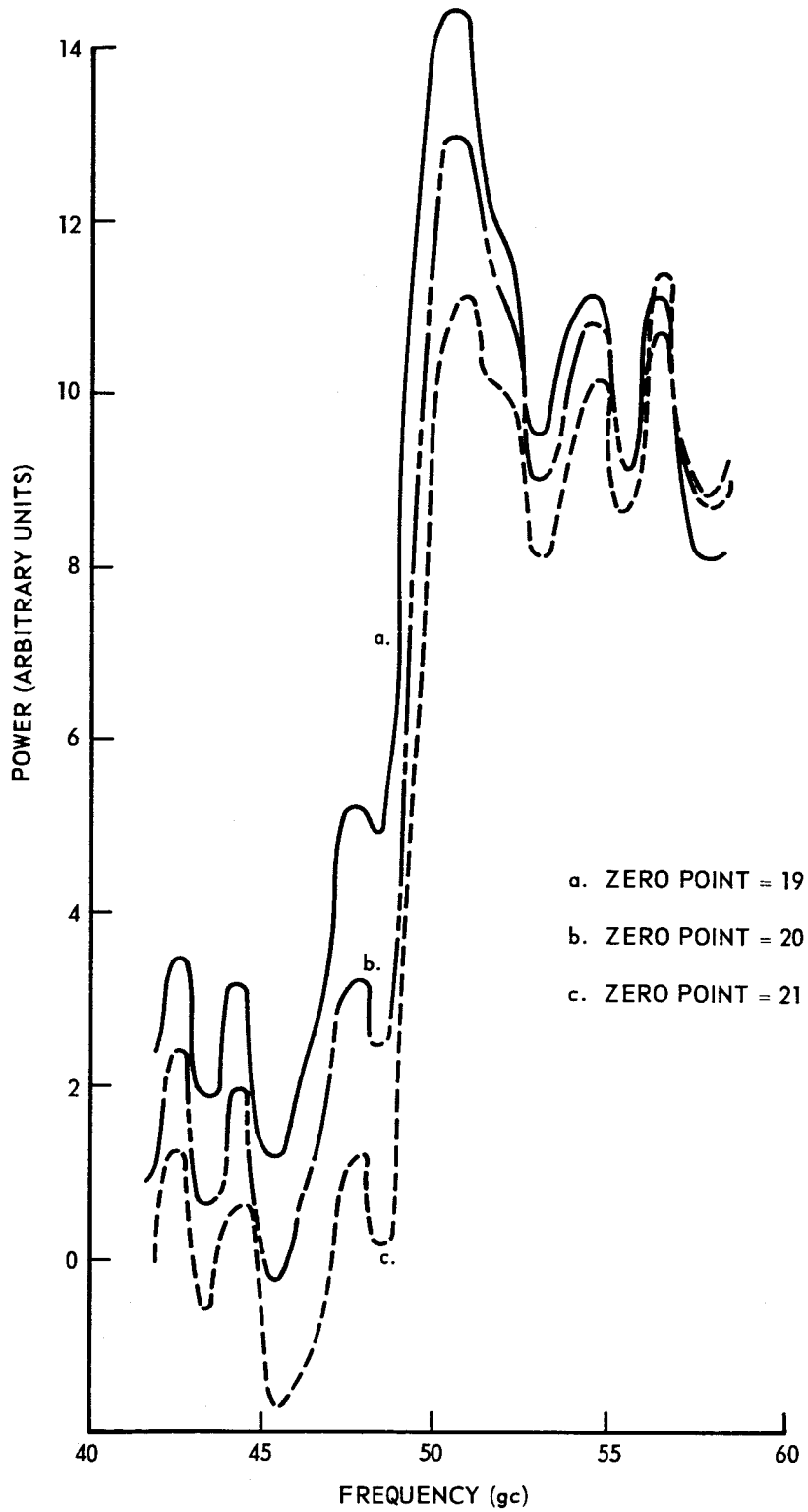

Figure 16. Effect of Variation of Zero Point of Interferogram on Filter Spectrum.